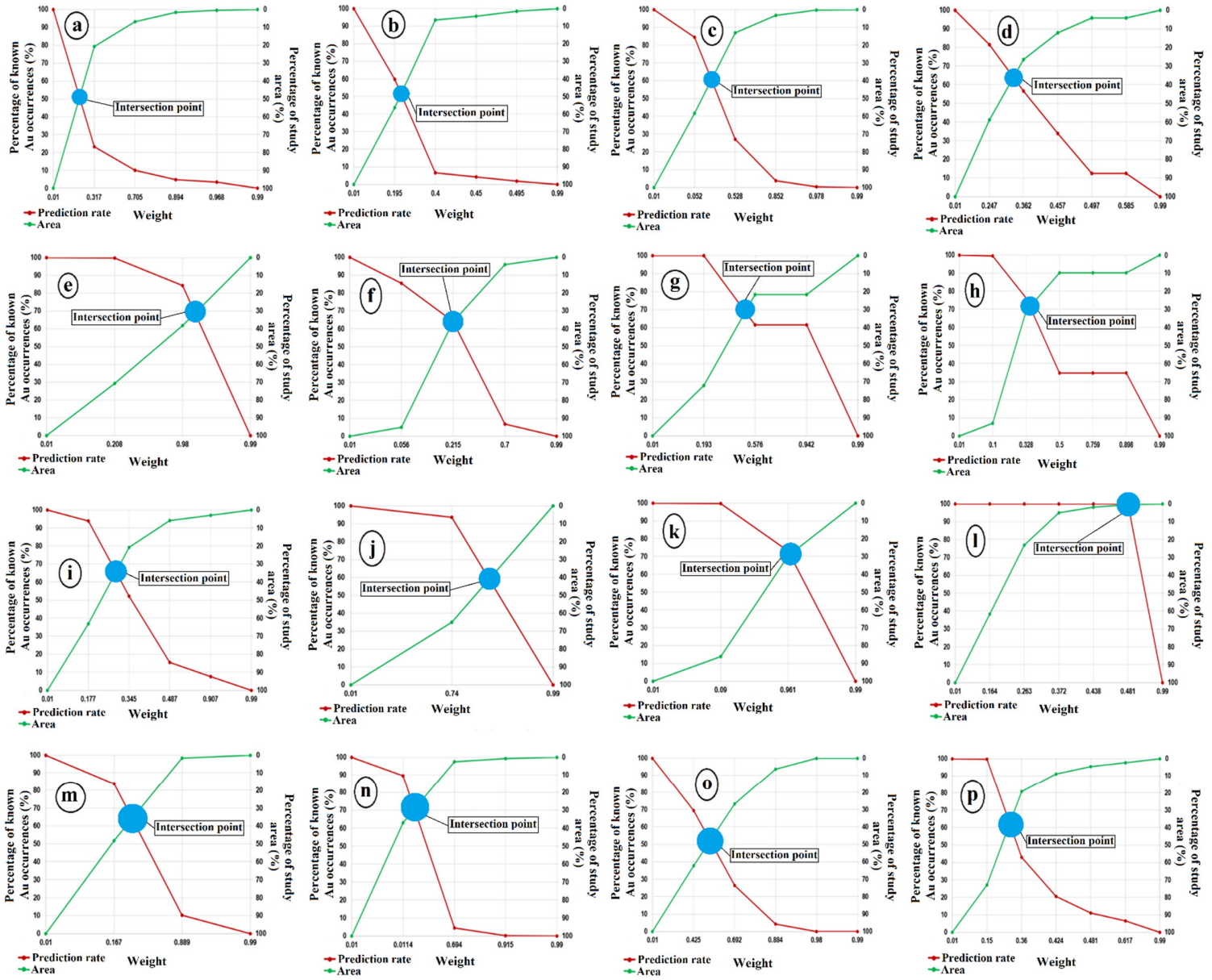

Figure S1. Prediction-area plots for the predictor maps used in this study, part 1: (a) density of Proterozoic dolerite dyke, (b) proximity to Proterozoic dolerite dykes, (c) density of principal faults, (d) proximity to principal faults, (e) proximity to greenstone belts, (f) proximity to siliciclastic and sedimentary rocks, (g) proximity to mafic–ultramafic volcanic rocks, (h) proximity to remotely sensed alteration systems, (i) proximity to 'high mag units', (j) proximity to felsic to intermediate volcanic rocks, (k) proximity to regional gravity highs, (l) proximity to known gold occurrences, (m) proximity to internal granitoids, (n) proximity to basement granitoids, (o) proximity to domains of juvenile crust (εNd-values of -0.2 to 2.4), and (p) proximity to areas of demagnetization.

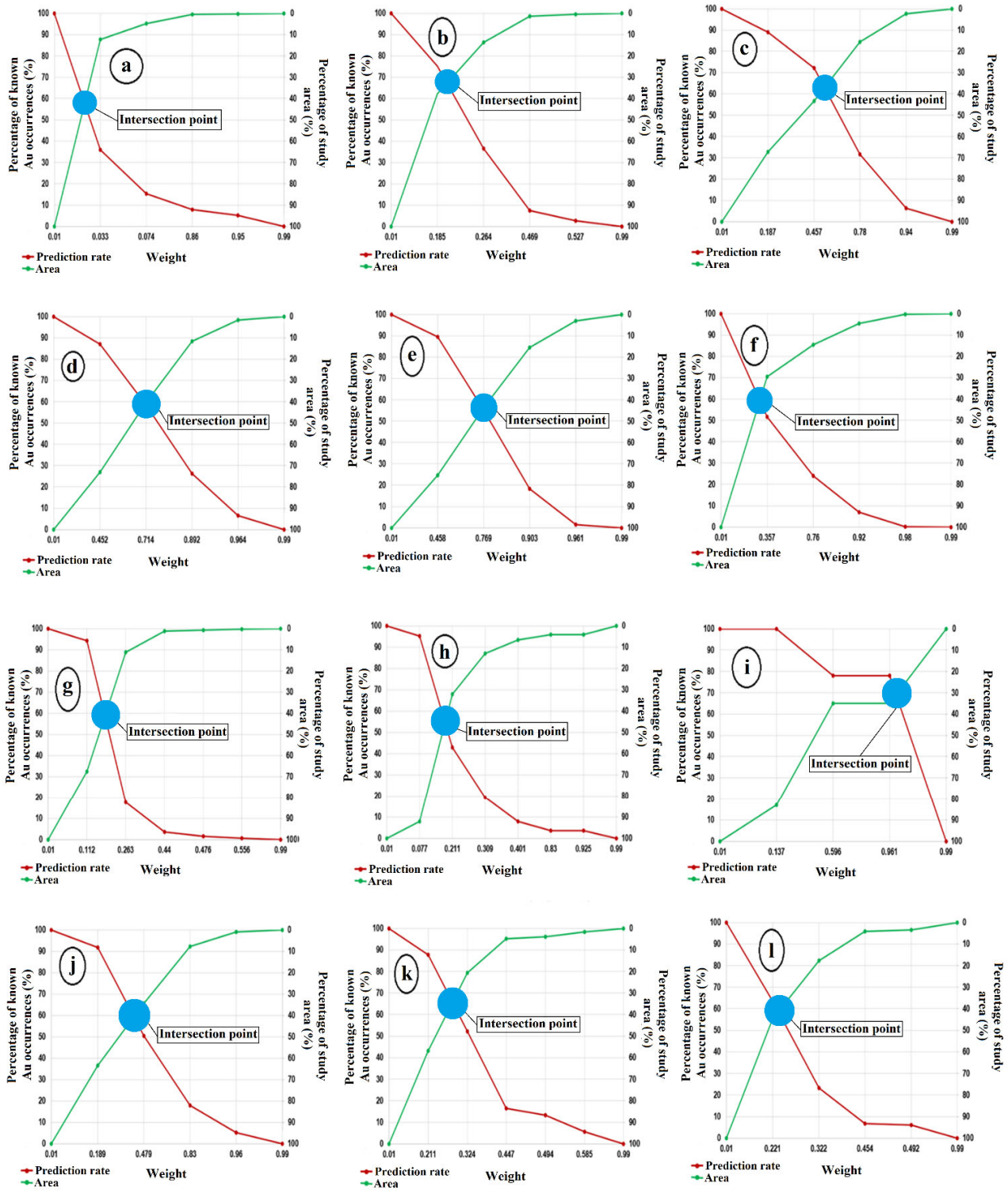

Figure S2. Prediction-area plots for the predictor maps used in this study, part 2: (a) density of lithological contacts, (b) proximity to lithological contacts, (c) density of ENE-WSW-striking gravity ridges, (d) density of ENE-WSW-striking gravity lineaments, (e) density of NNW-SSE-striking gravity lineaments, (f) density of principal fault intersections, (g) proximity to fold hinges, (h) proximity to domains of high K/Th values (≥95th percentile), (i) proximity to domains of favorable metamorphic grade, (j) density of NNW-SSE-striking gravity ridges, (k) proximity to subsidiary faults, and (l) proximity to flanks of granitoid bodies.

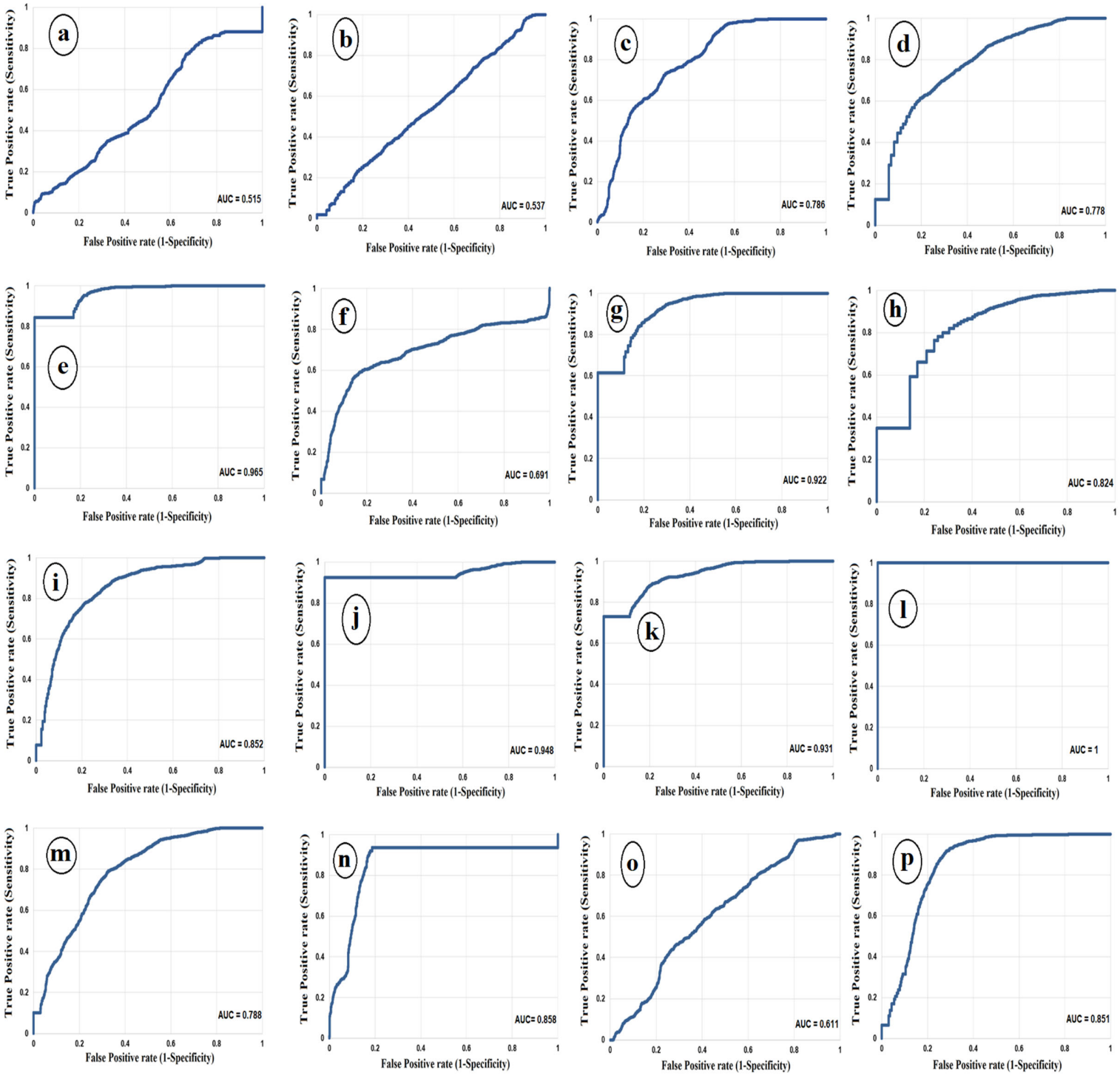

Figure S3. Receiver operating characteristic curves for the predictor maps used in this study, part 1: (a) density of Proterozoic dolerite dyke, (b) proximity to Proterozoic dolerite dykes, (c) density of principal faults, (d) proximity to principal faults, (e) proximity to greenstone belts, (f) proximity to siliciclastic and sedimentary rocks, (g) proximity to mafic–ultramafic volcanic rocks, (h) proximity to remotely sensed alteration systems, (i) proximity to 'high mag units', (j) proximity to felsic to intermediate volcanic rocks, (k) proximity to regional gravity highs, (l) proximity to known gold occurrences, (m) proximity to internal granitoids, (n) proximity to basement granitoids, (o) proximity to domains of juvenile crust (εNd-values of -0.2 to 2.4), and (p) proximity to areas of demagnetization.

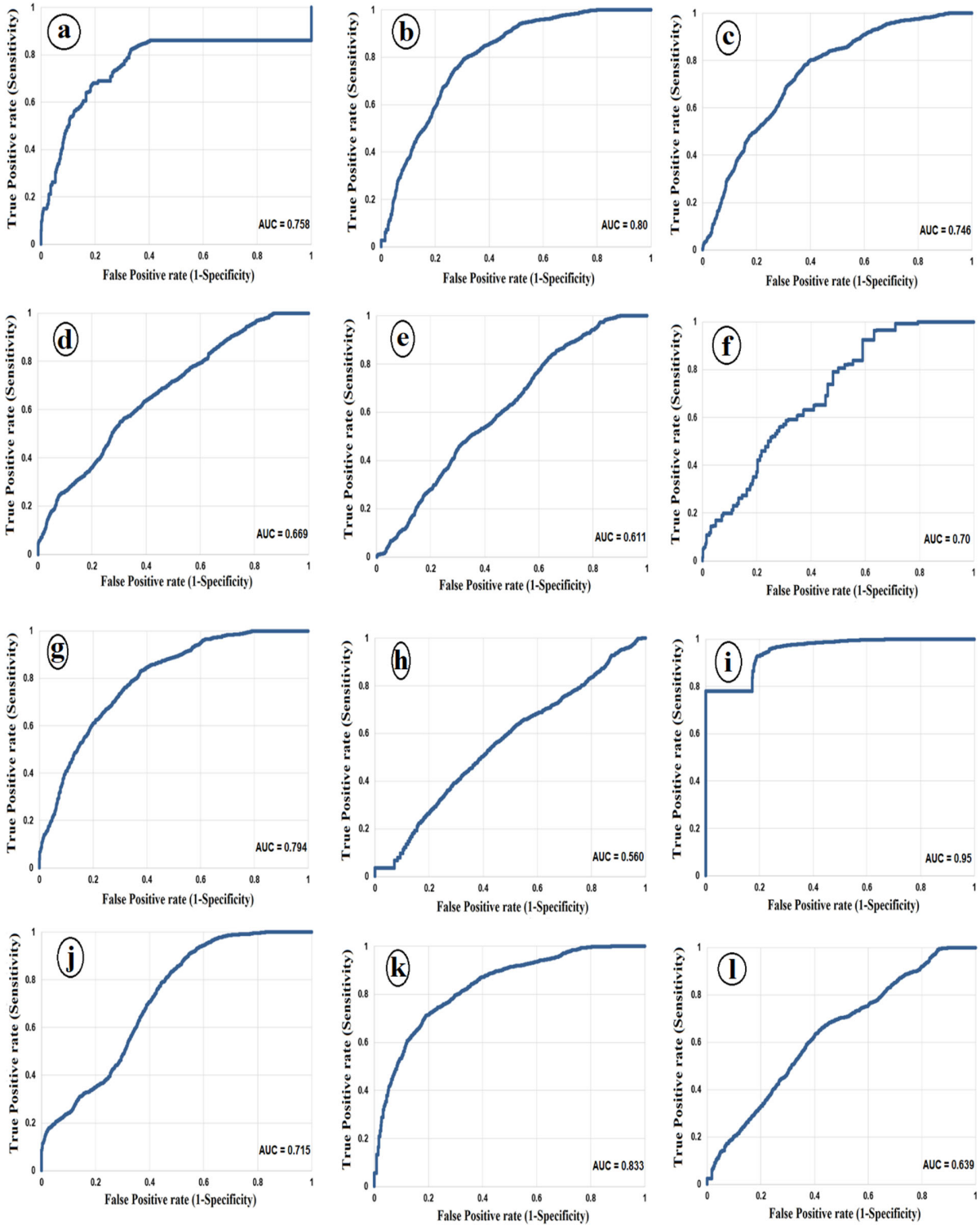

Figure S4. Figure S3: Receiver operating characteristic curves for the predictor maps used in this study, part 2: (a) density of lithological contacts, (b) proximity to lithological contacts, (c) density of ENE-WSW-striking gravity ridges, (d) density of ENE-WSW-striking gravity lineaments, (e) density of NNW-SSE-striking gravity lineaments, (f) density of principal fault intersections, (g) proximity to fold hinges, (h) proximity to domains of high K/Th values (≥95th percentile), (i) proximity to domains of favorable metamorphic grade, (j) density of NNW-SSE-striking gravity ridges, (k) proximity to subsidiary faults, and (l) proximity to flanks of granitoid bodies.

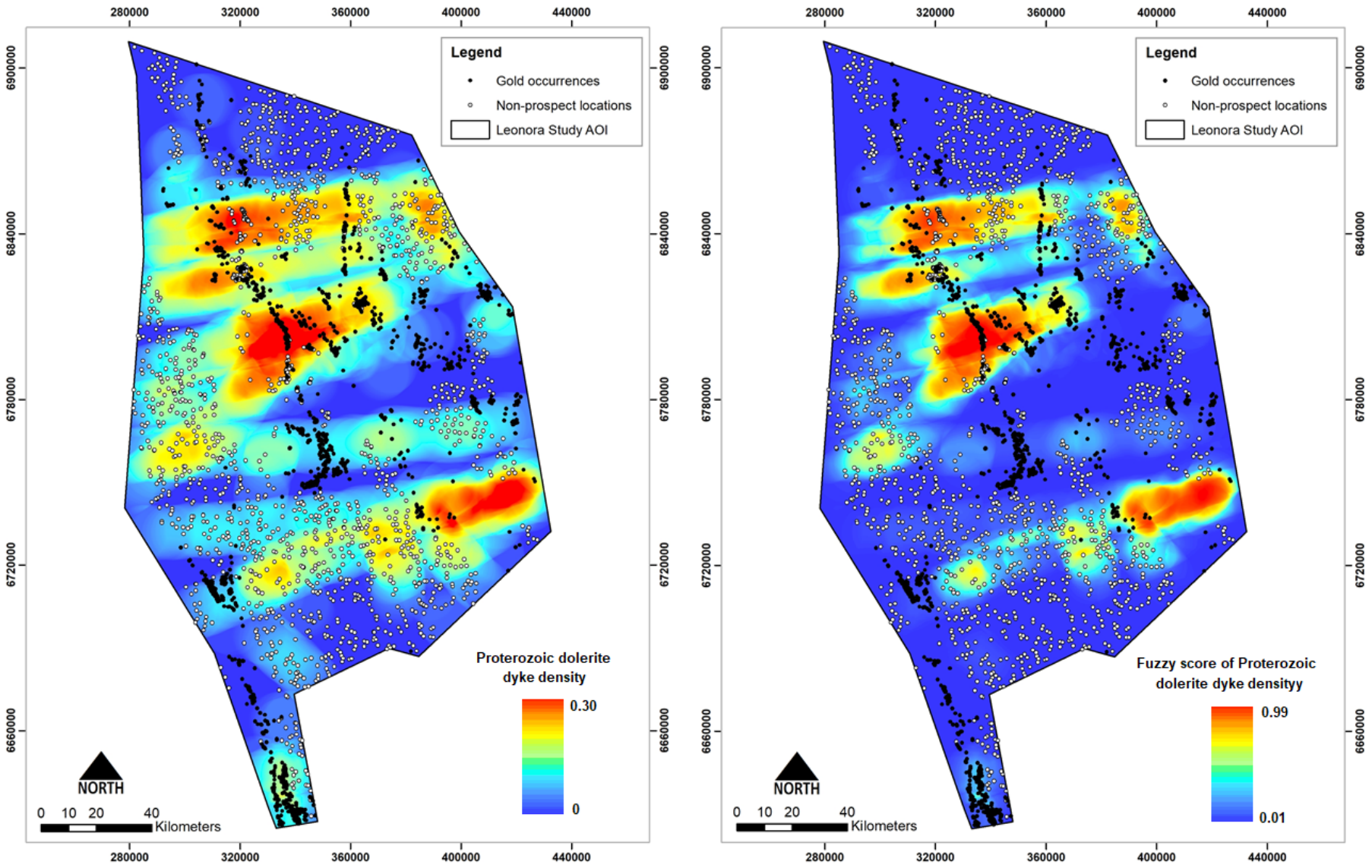

Figure S5. Predictor maps used in this study, part 1: (a) density of Proterozoic dolerite dykes, and (b) density of Proterozoic dolerite dykes, continuously weighted.

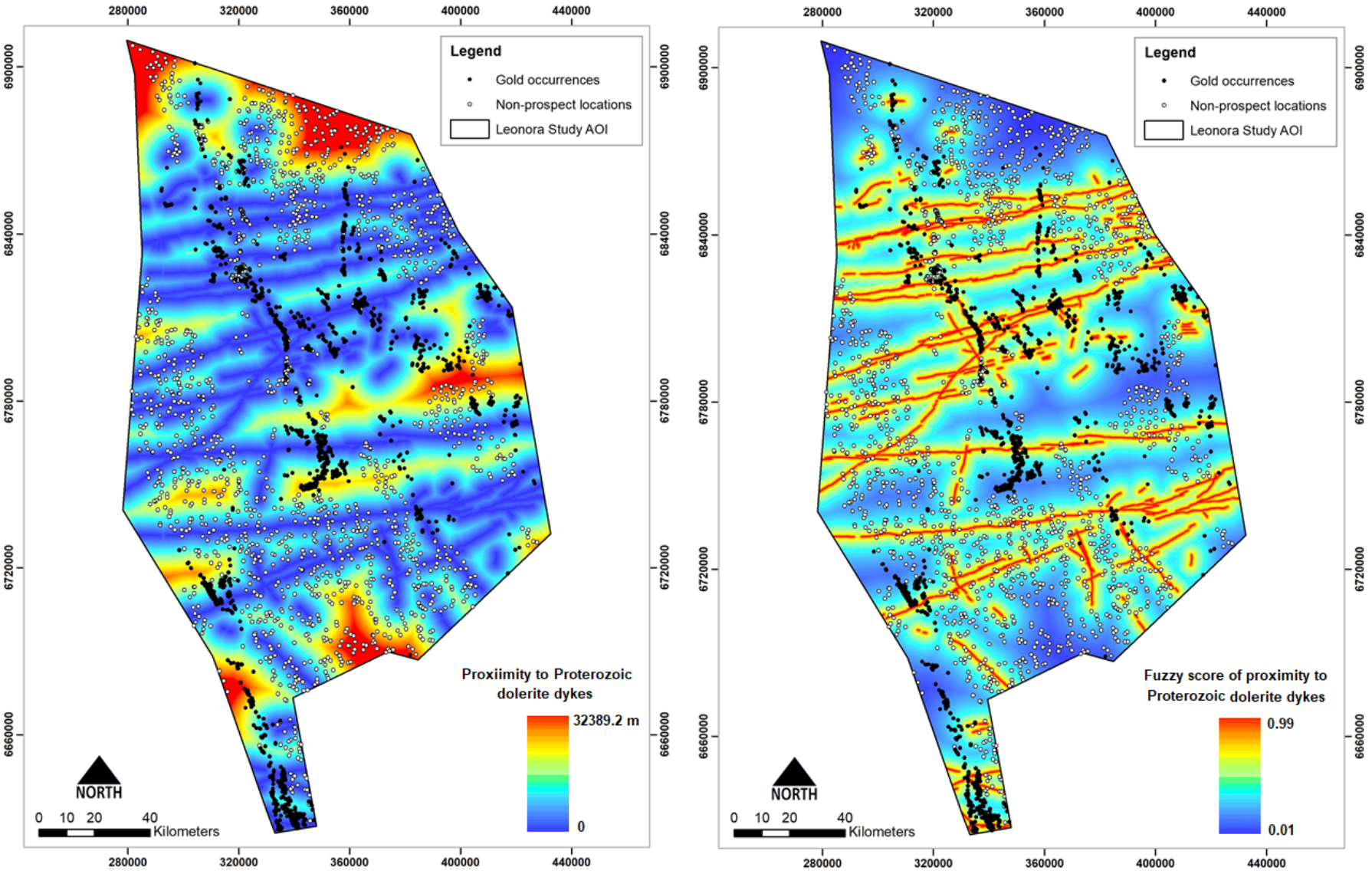

Figure S6. Predictor maps used in this study, part 2: (a) proximity to Proterozoic dolerite dykes, and (b) proximity to Proterozoic dolerite dykes, continuously weighted.

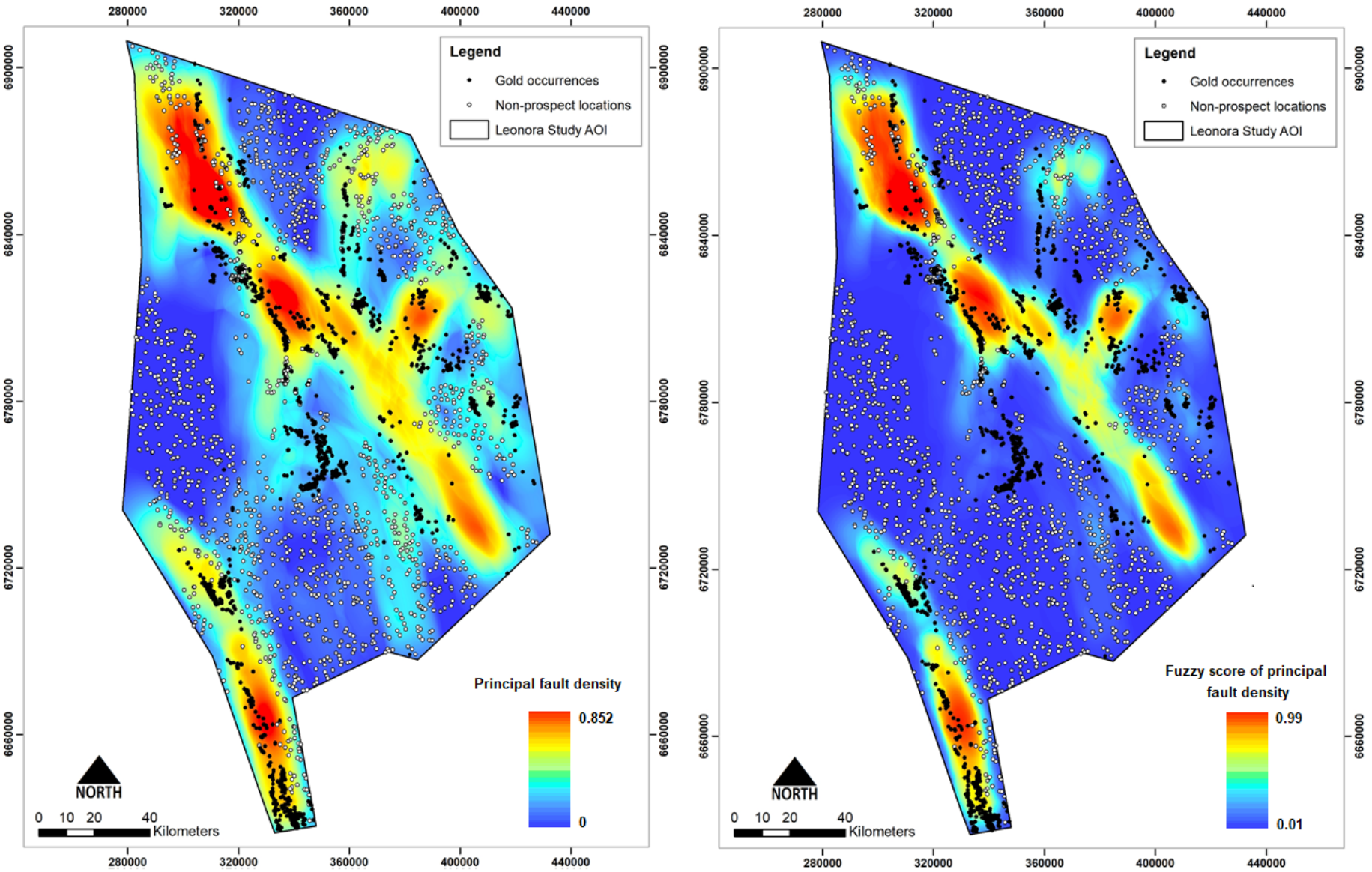

Figure S7. Predictor maps used in this study, part 3: (a) density of principal faults, and (b) density of principal faults, continuously weighted.

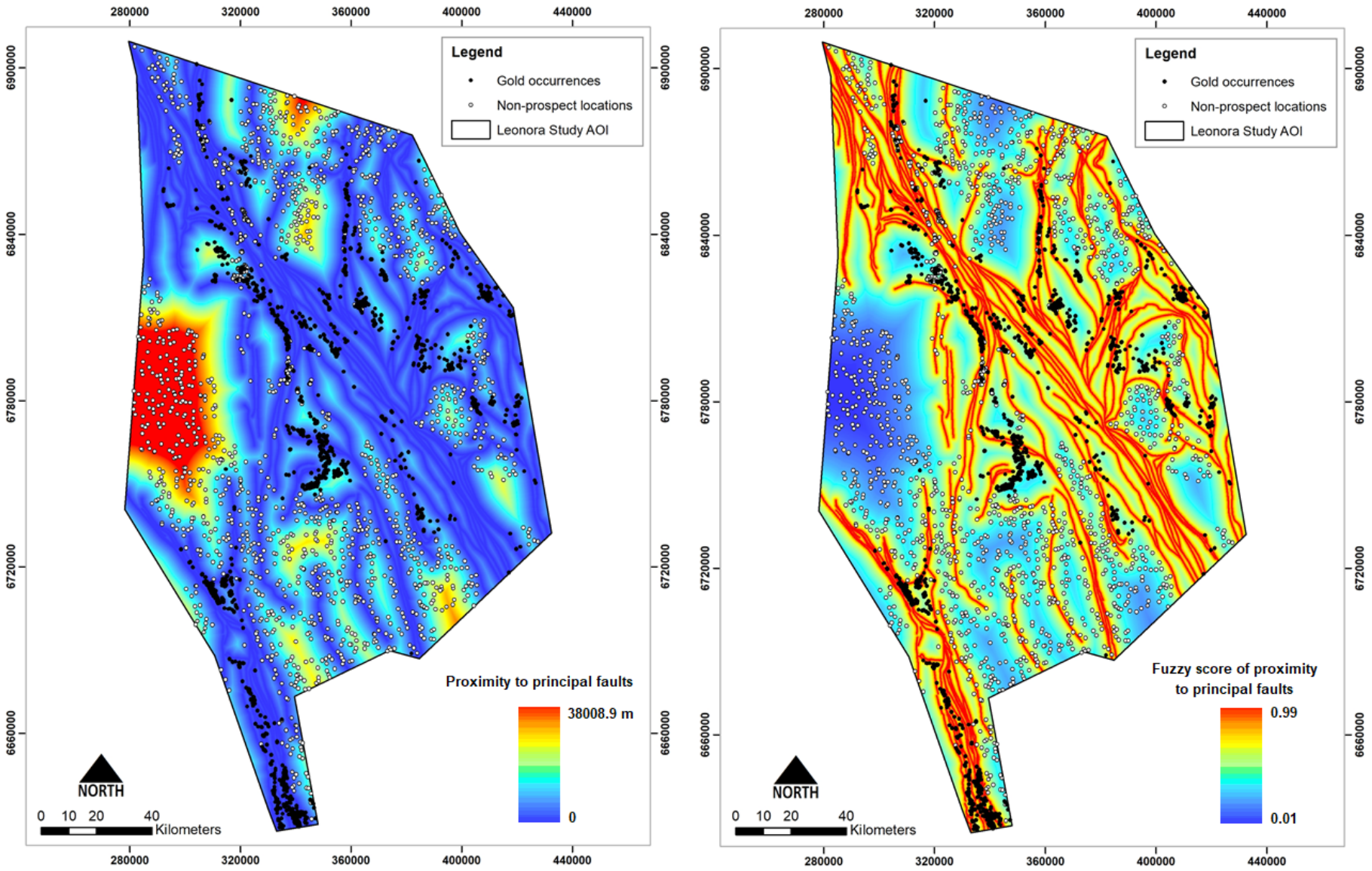

Figure S8. Predictor maps used in this study, part 4: (a) proximity to principal faults, and (b) proximity to principal faults, continuously weighted.

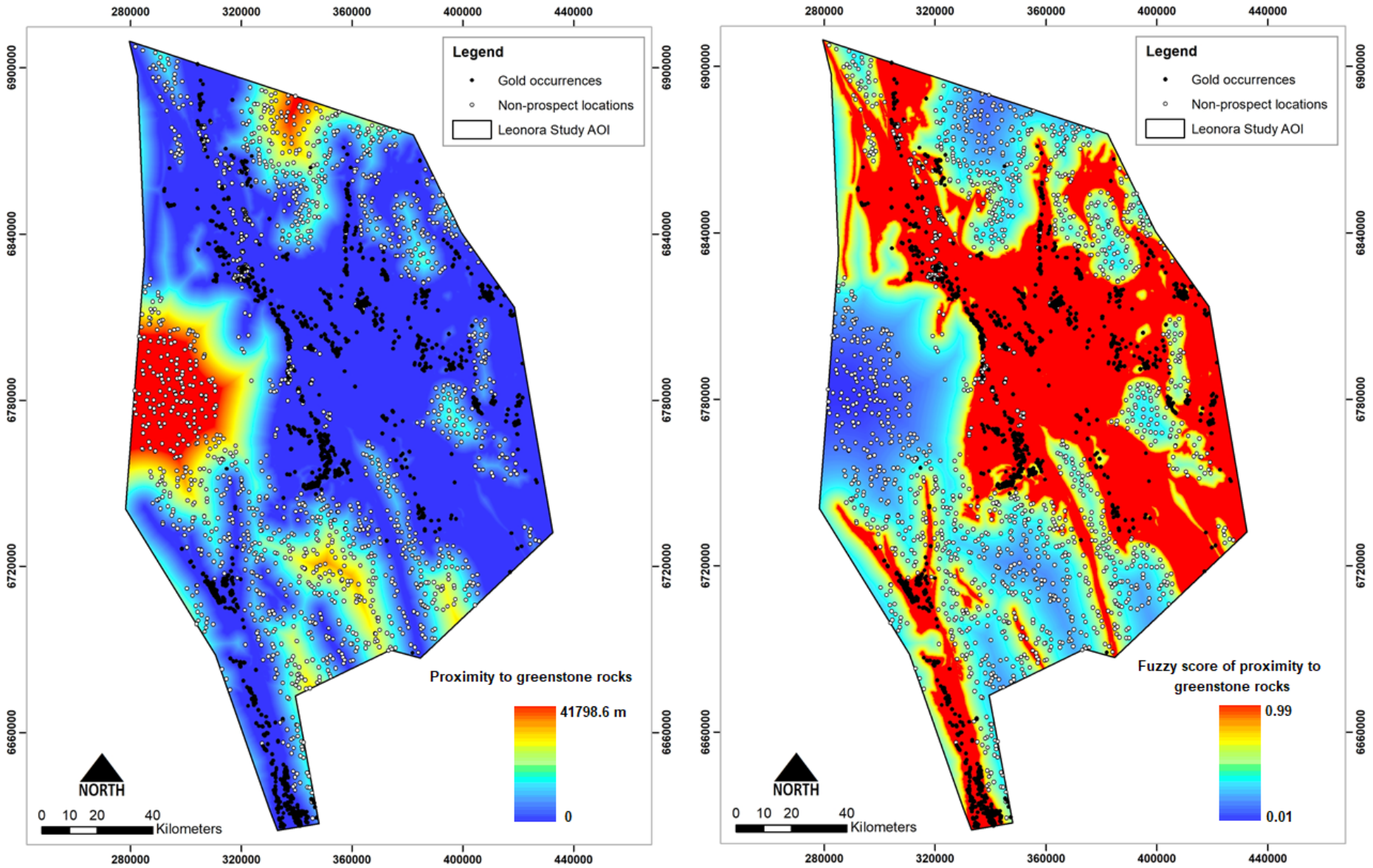

Figure S9. Predictor maps used in this study, part 5: (a) proximity to greenstone belts, and (b) proximity to greenstone belts, continuously weighted.

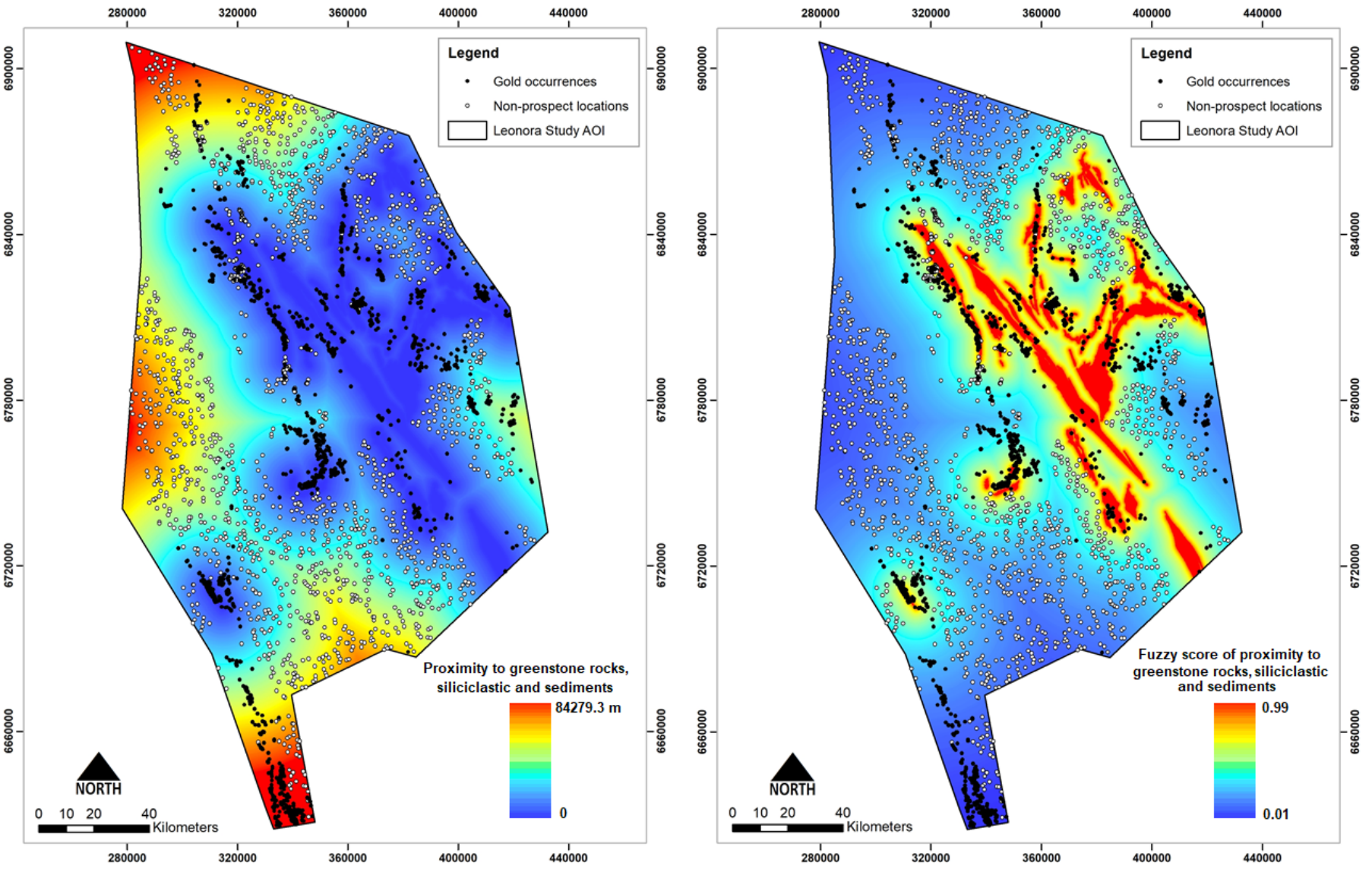

Figure S10. Predictor maps used in this study, part 6: (a) proximity to siliciclastic and sedimentary rocks, and (b) proximity to siliciclastic and sedimentary rocks, continuously weighted.

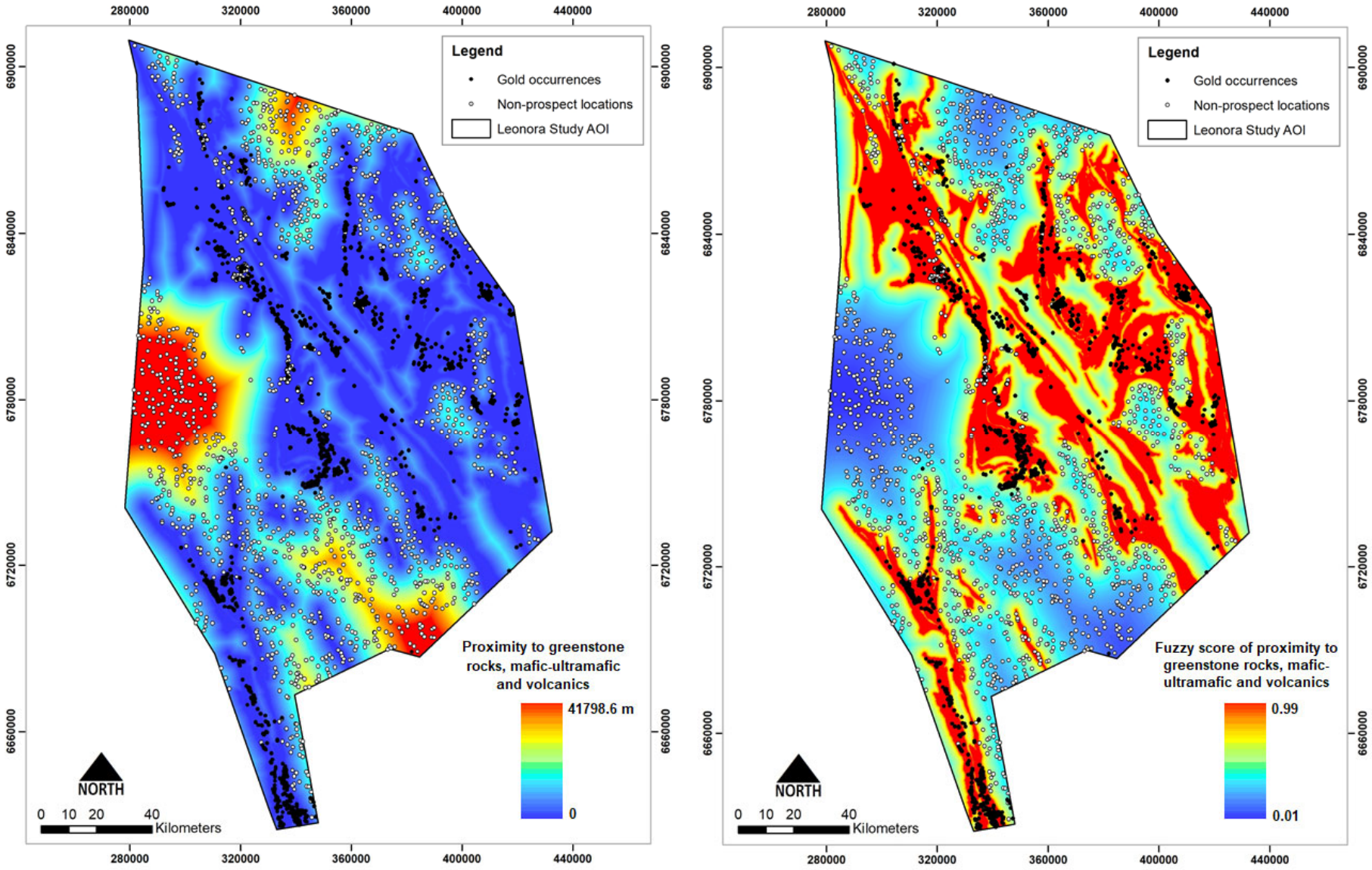

Figure S11. Predictor maps used in this study, part 7: (a) oroximity to mafic–ultramafic volcanic rocks, and (b) proximity to mafic–ultramafic volcanic rocks, continuously weighted.

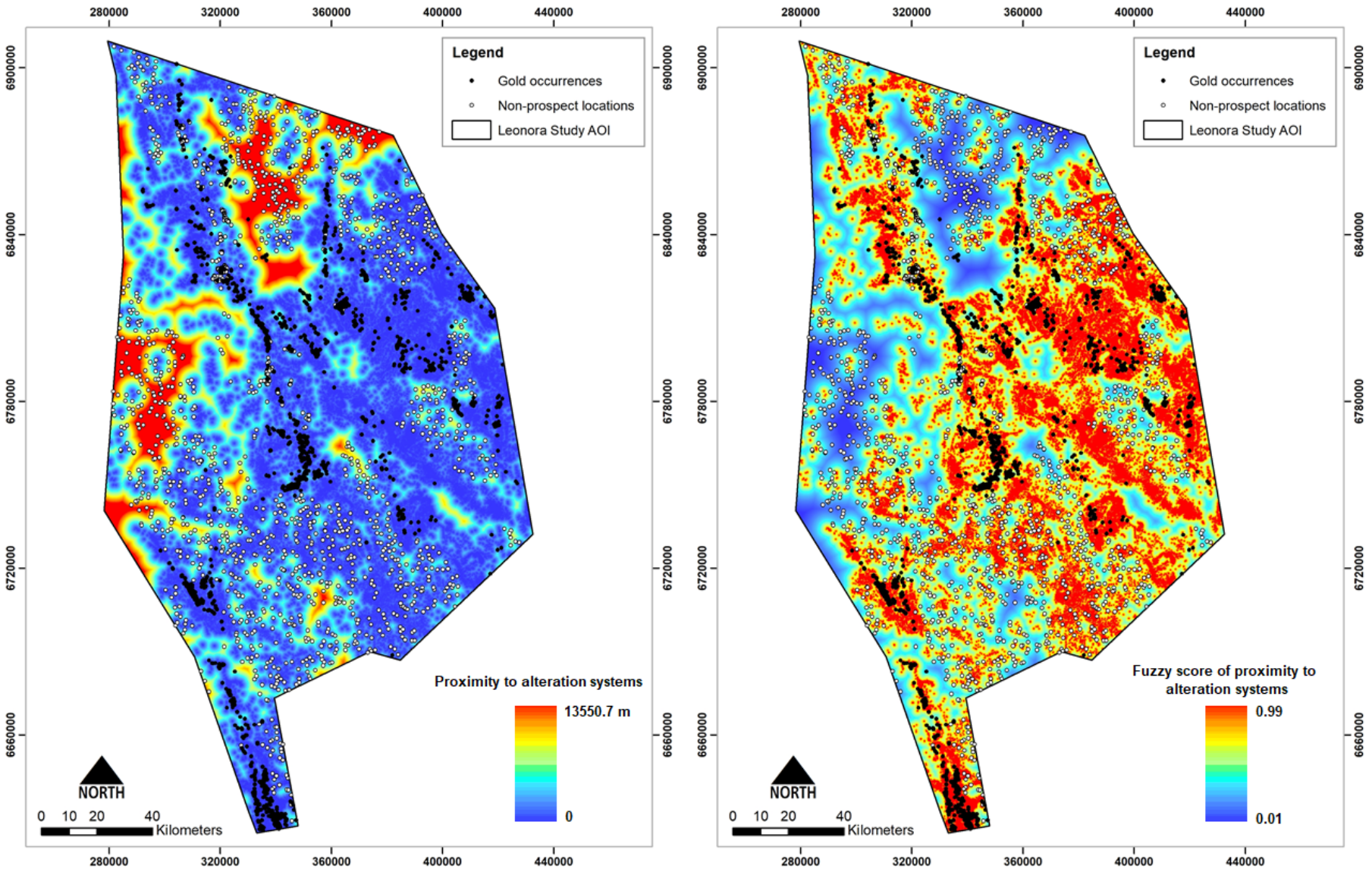

Figure S12. Predictor maps used in this study, part 8: (a) proximity to remotely sensed alteration systems, and (b) proximity to remotely sensed alteration systems, continuously weighted.

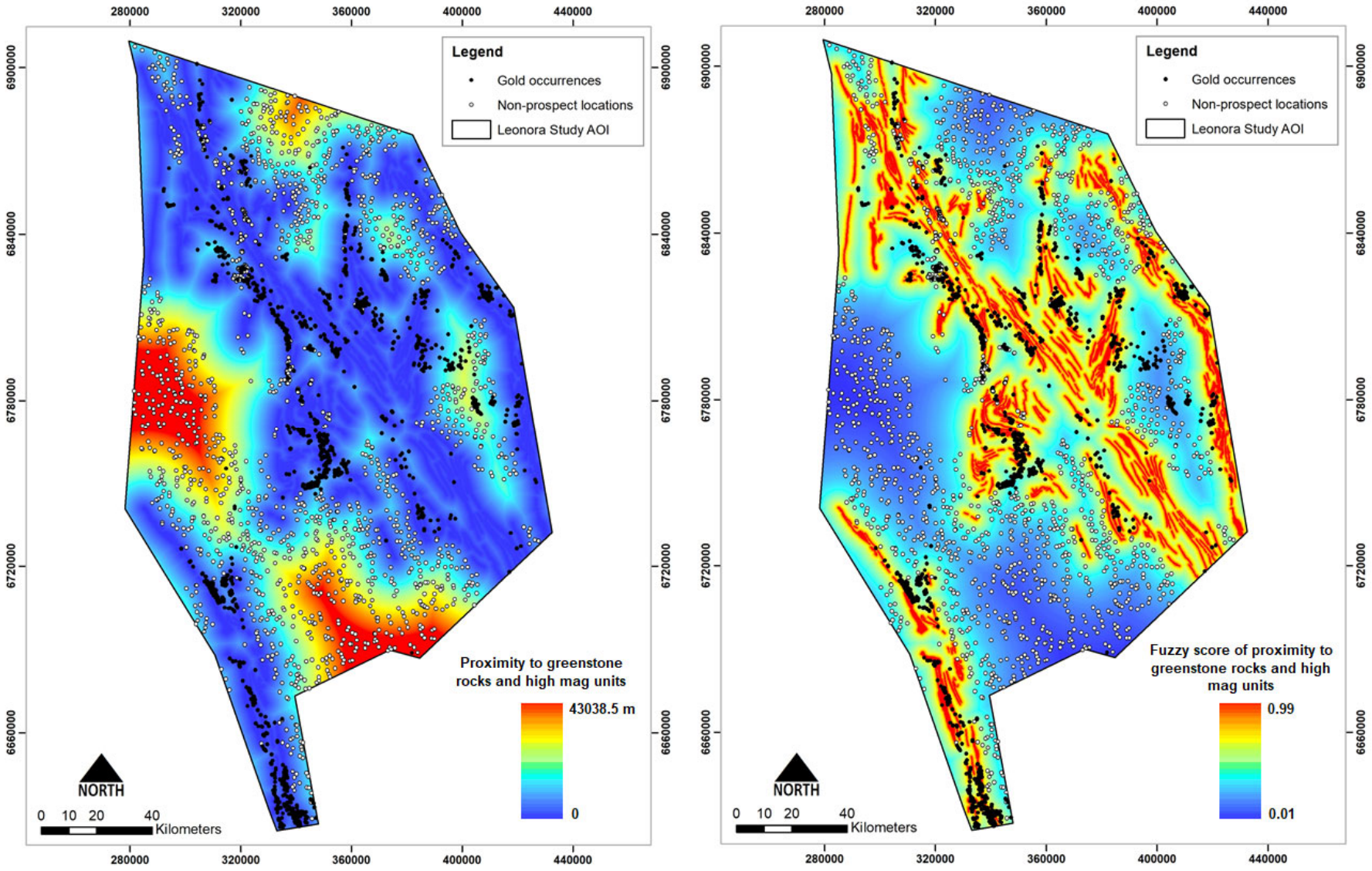

Figure S13. Predictor maps used in this study, part 9: (a) proximity to 'high mag units', and (b) proximity to 'high mag units', continuously weighted.

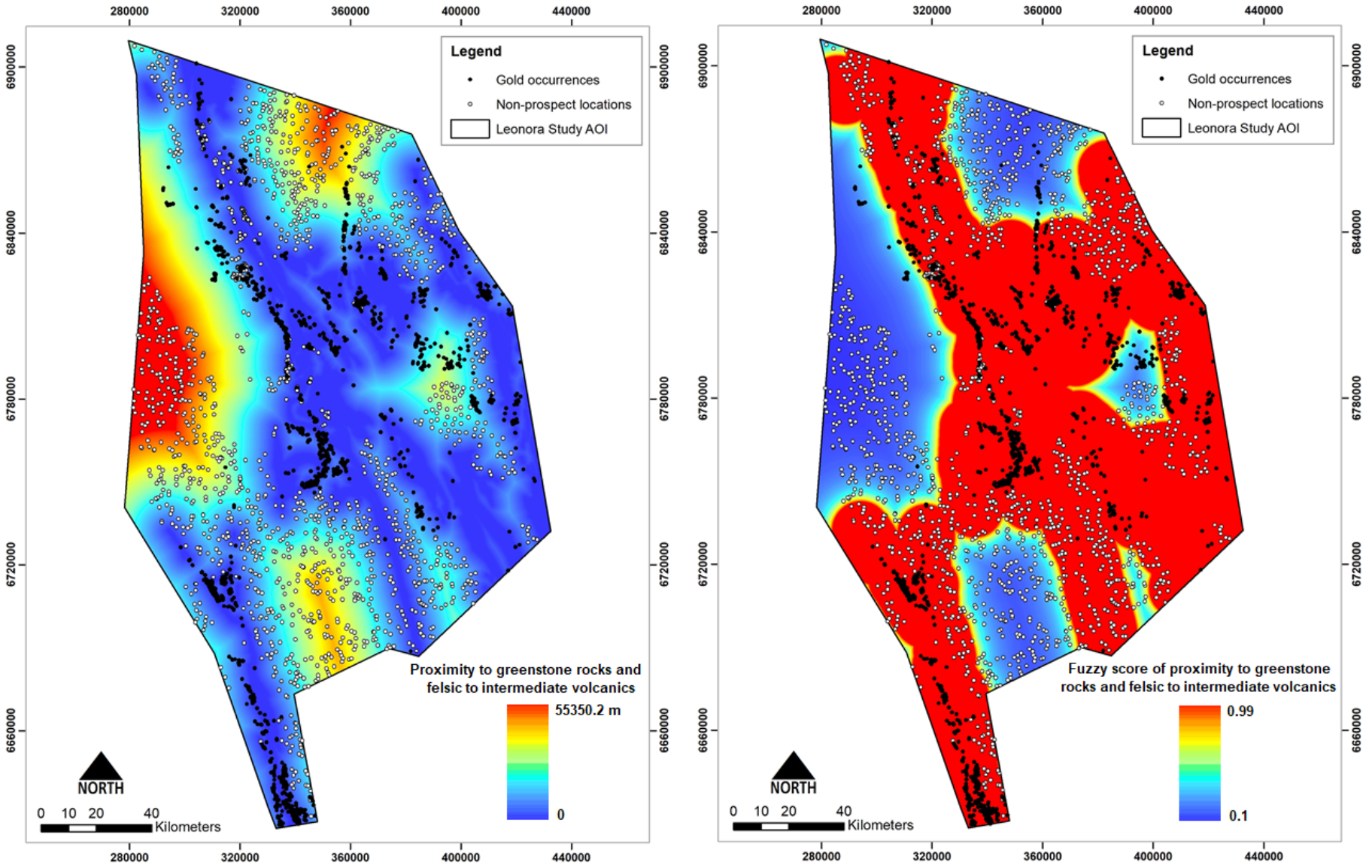

Figure S14. Predictor maps used in this study, part 10: (a) proximity to felsic to intermediate volcanic rocks, and (b) proximity to felsic to intermediate volcanic rocks, continuously weighted.

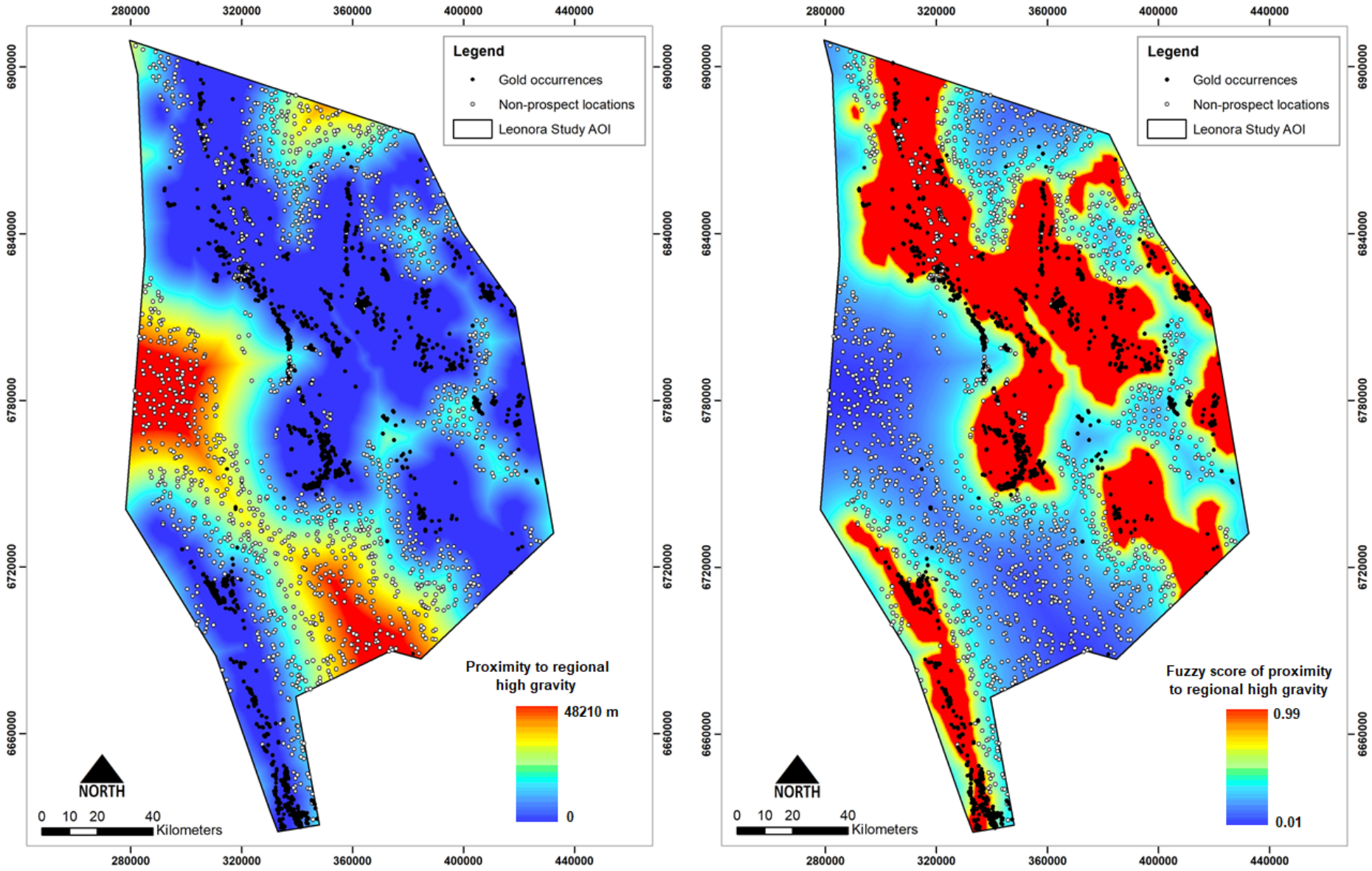

Figure S15. Predictor maps used in this study, part 11: (a) proximity to regional gravity highs, and (b) proximity to regional gravity highs, continuously weighted.

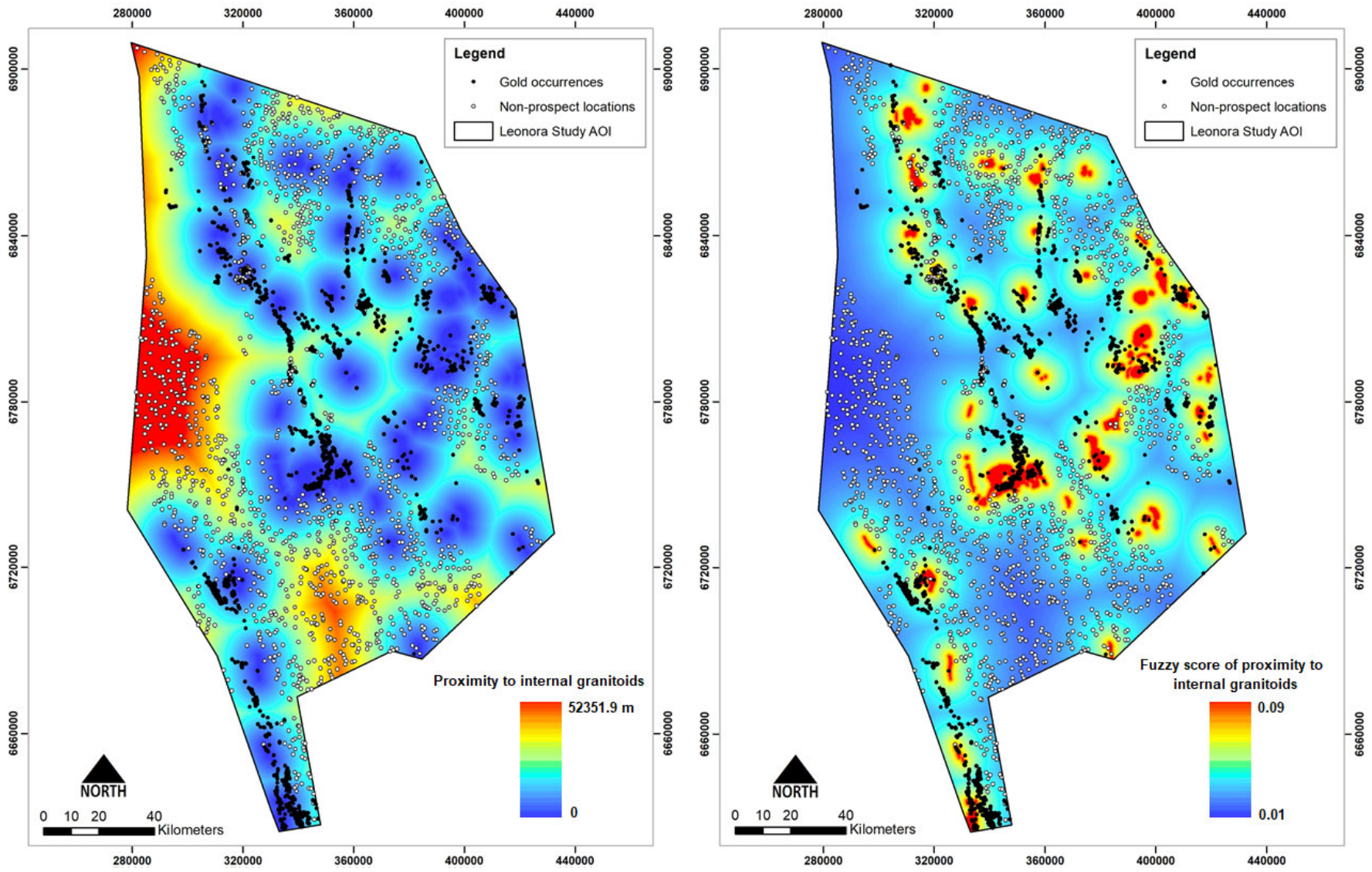

Figure S16. Predictor maps used in this study, part 12: (a) proximity to internal granitoids, and (b) proximity to internal granitoids, continuously weighted.

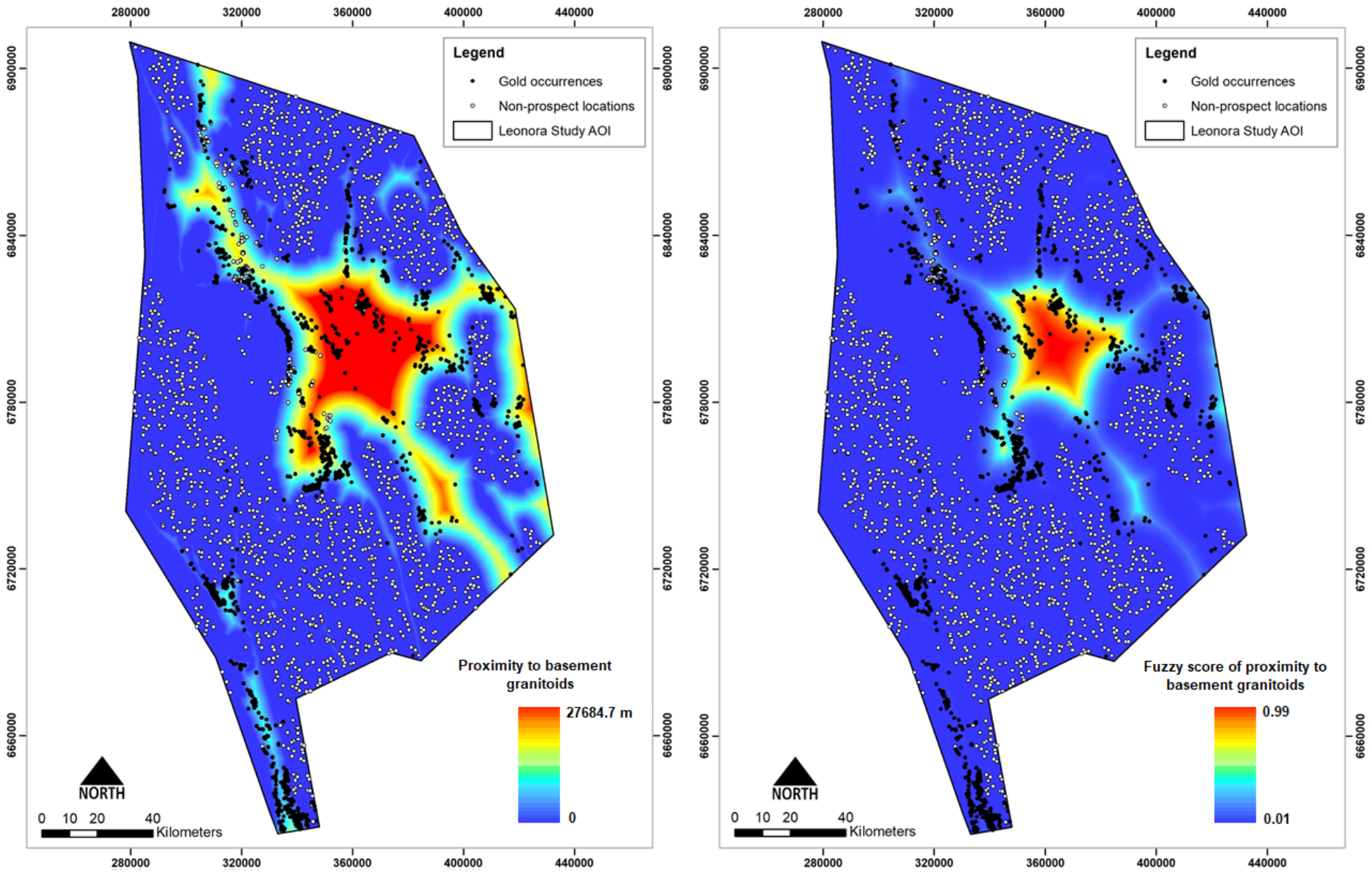

Figure S17. Predictor maps used in this study, part 13: (a) proximity to basement granitoids, and (b) proximity to basement granitoids, continuously weighted.

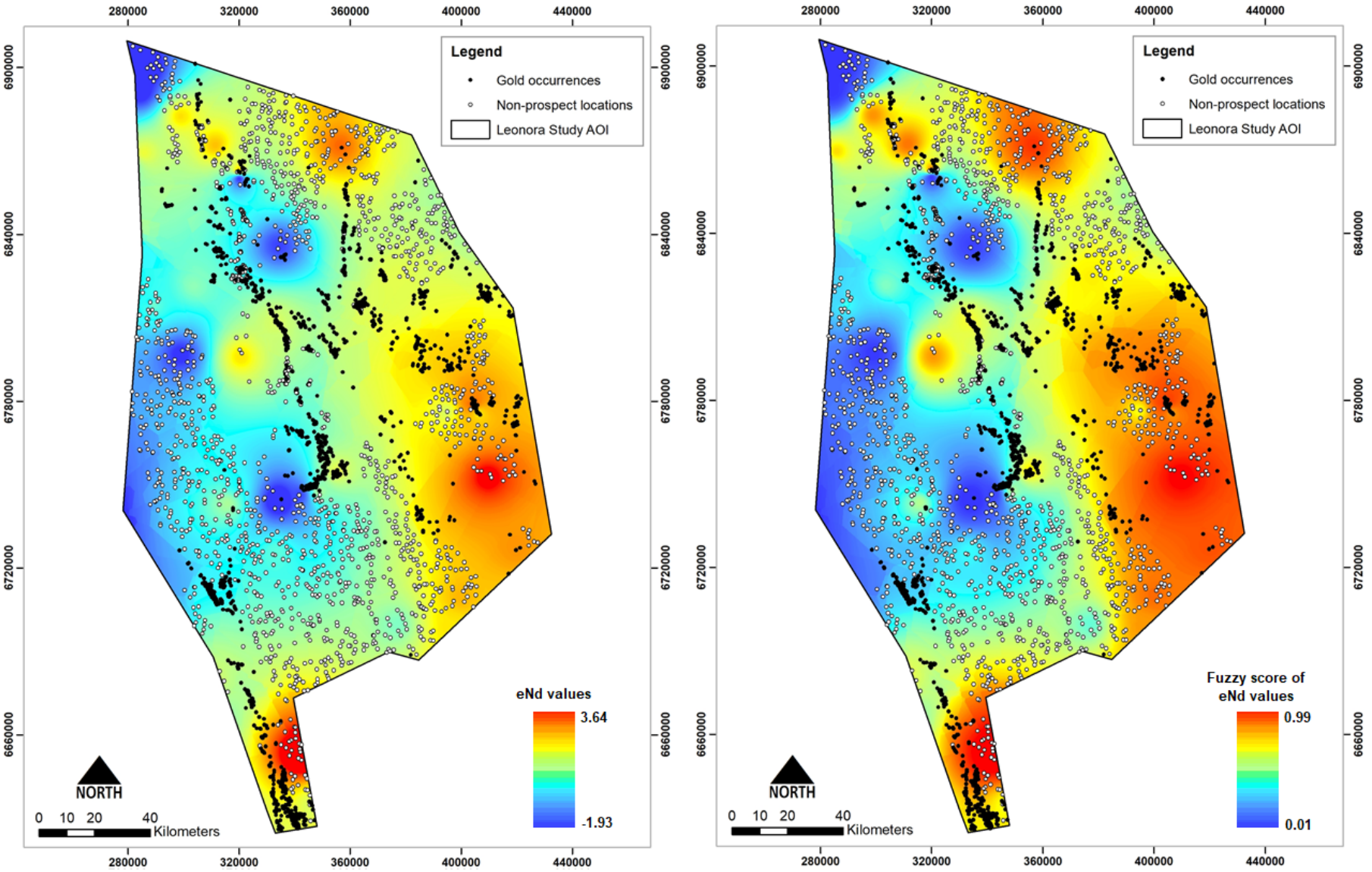

Figure S18. Predictor maps used in this study, part 14: (a) proximity to domains of juvenile crust (εNd-values of -0.2 to 2.4), and (b) proximity to domains of juvenile crust (εNd-values of -0.2 to 2.4), continuously weighted.

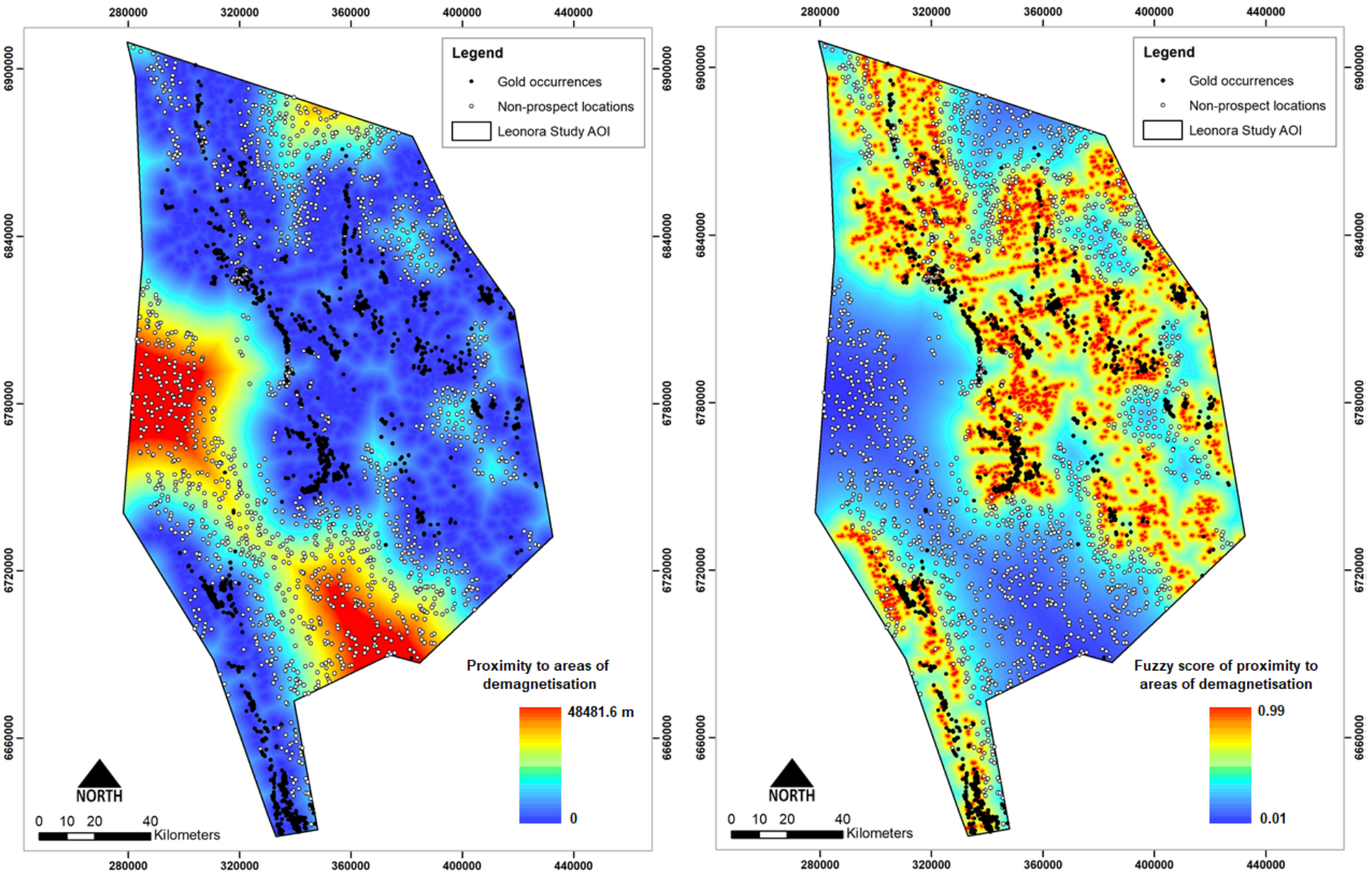

Figure S19. Predictor maps used in this study, part 15: (a) proximity to areas of demagnetization, and (b) proximity to areas of demagnetization, continuously weighted.

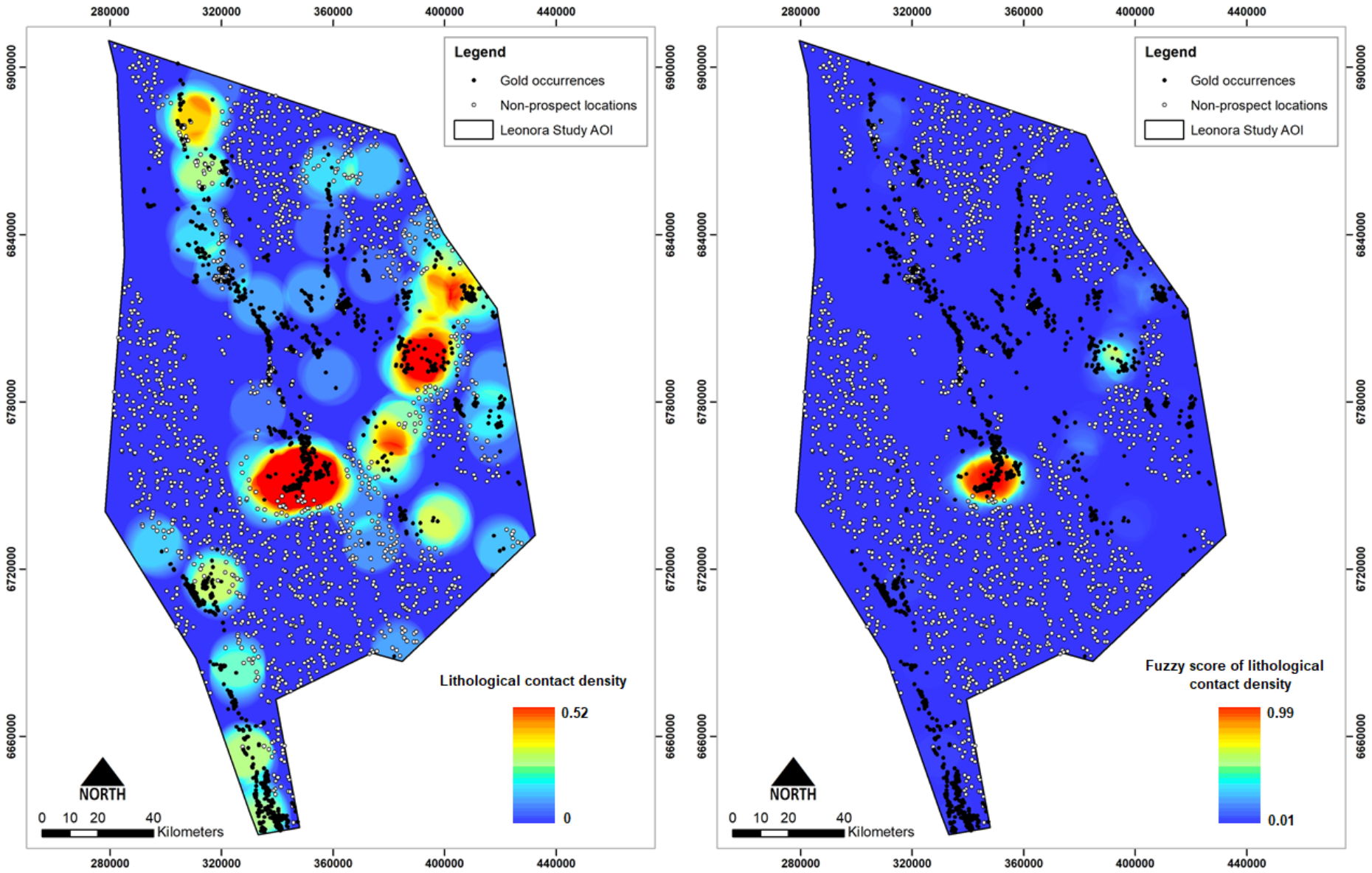

Figure S20. Predictor maps used in this study, part 16: (a) density of lithological contacts, and (b) density of lithological contacts, continuously weighted.

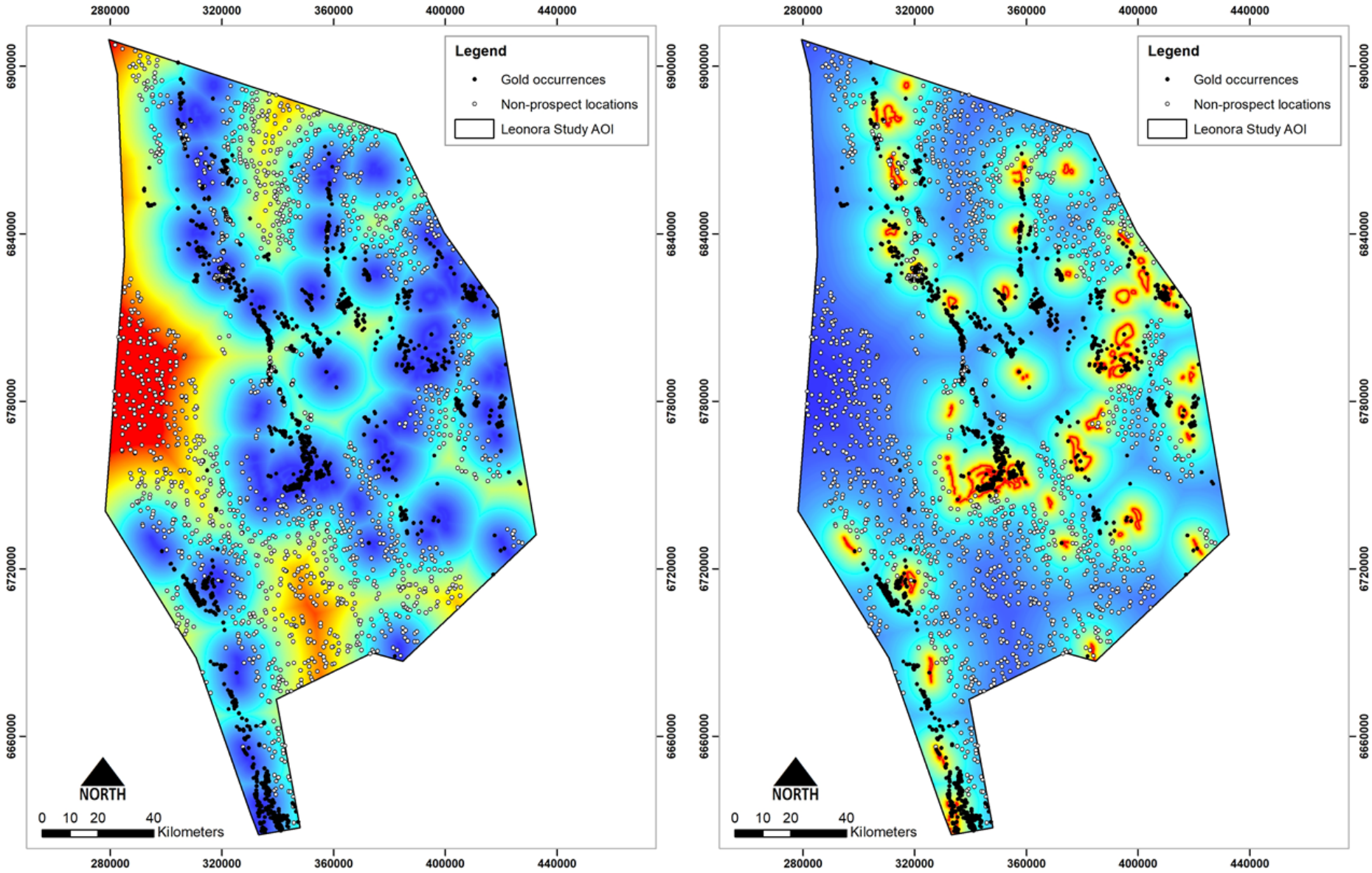

Figure S21. Predictor maps used in this study, part 17: (a) proximity to lithological contacts, and (b) proximity to lithological contacts, continuously weighted.

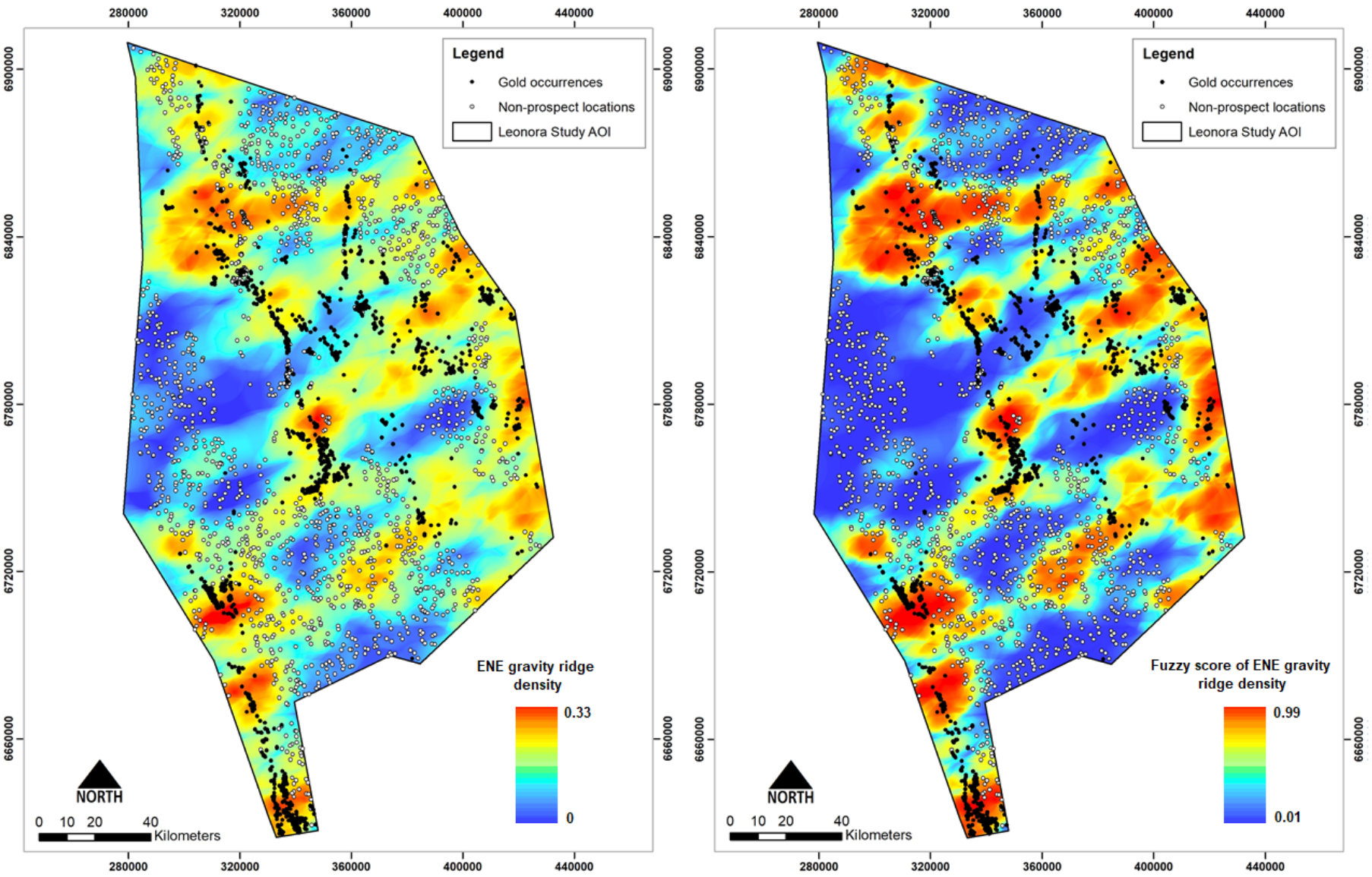

Figure S22. Predictor maps used in this study, part 18: (a) density of ENE-WSW-striking gravity ridges, and (b) density of ENE-WSW-striking gravity ridges, continuously weighted.

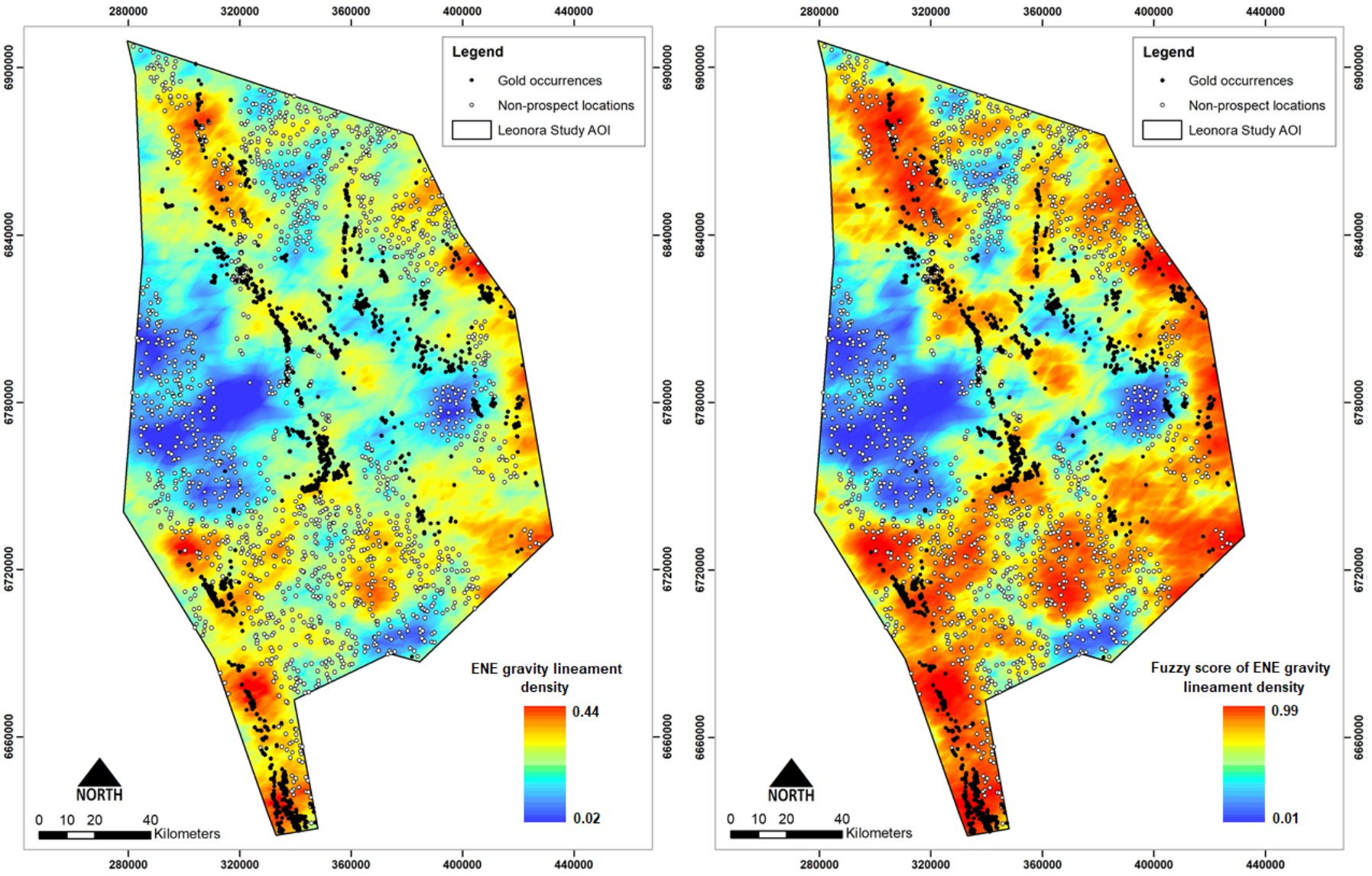

Figure S23. Predictor maps used in this study, part 19: (a) density of ENE-WSW-striking gravity lineaments, and (b) density of ENE-WSW-striking gravity lineaments, continuously weighted.

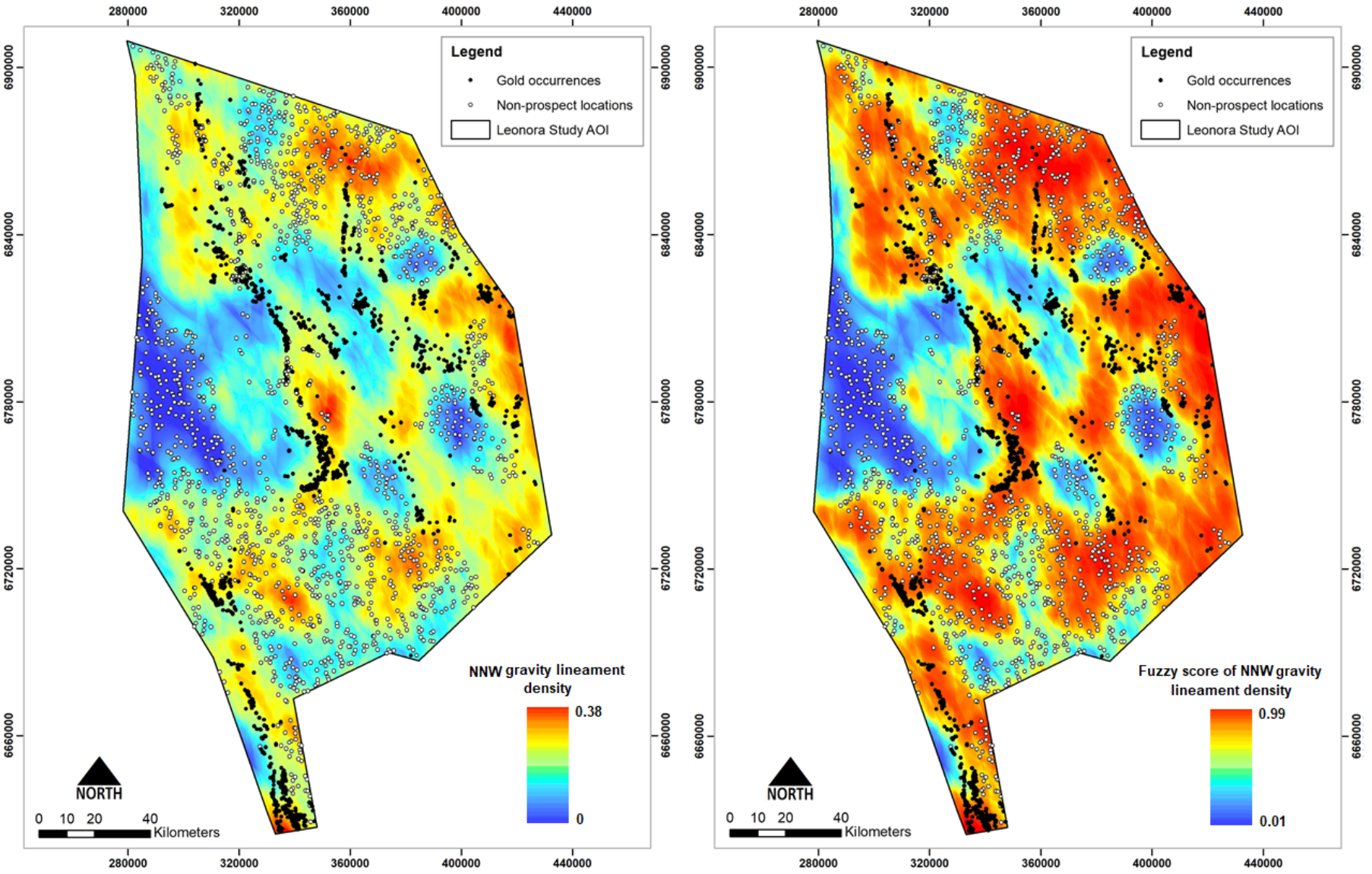

Figure S24. Predictor maps used in this study, part 20: (a) density of NNW-SSE-striking gravity lineaments, and (b) density of NNW-SSE-striking gravity lineaments, continuously weighted.

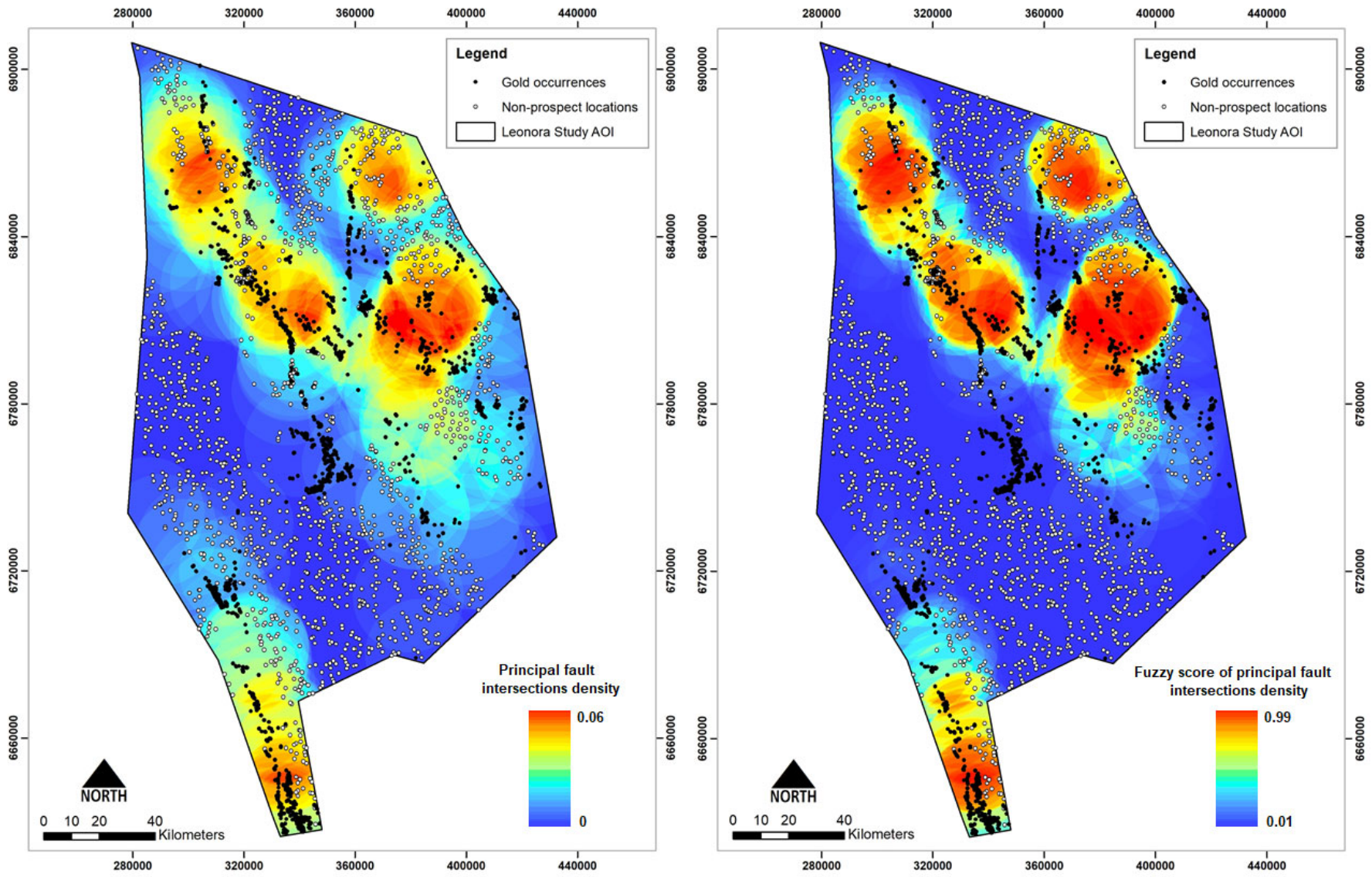

Figure S25. Predictor maps used in this study, part 21: (a) density of principal fault intersections, and (b) density of principal fault intersections, continuously weighted.

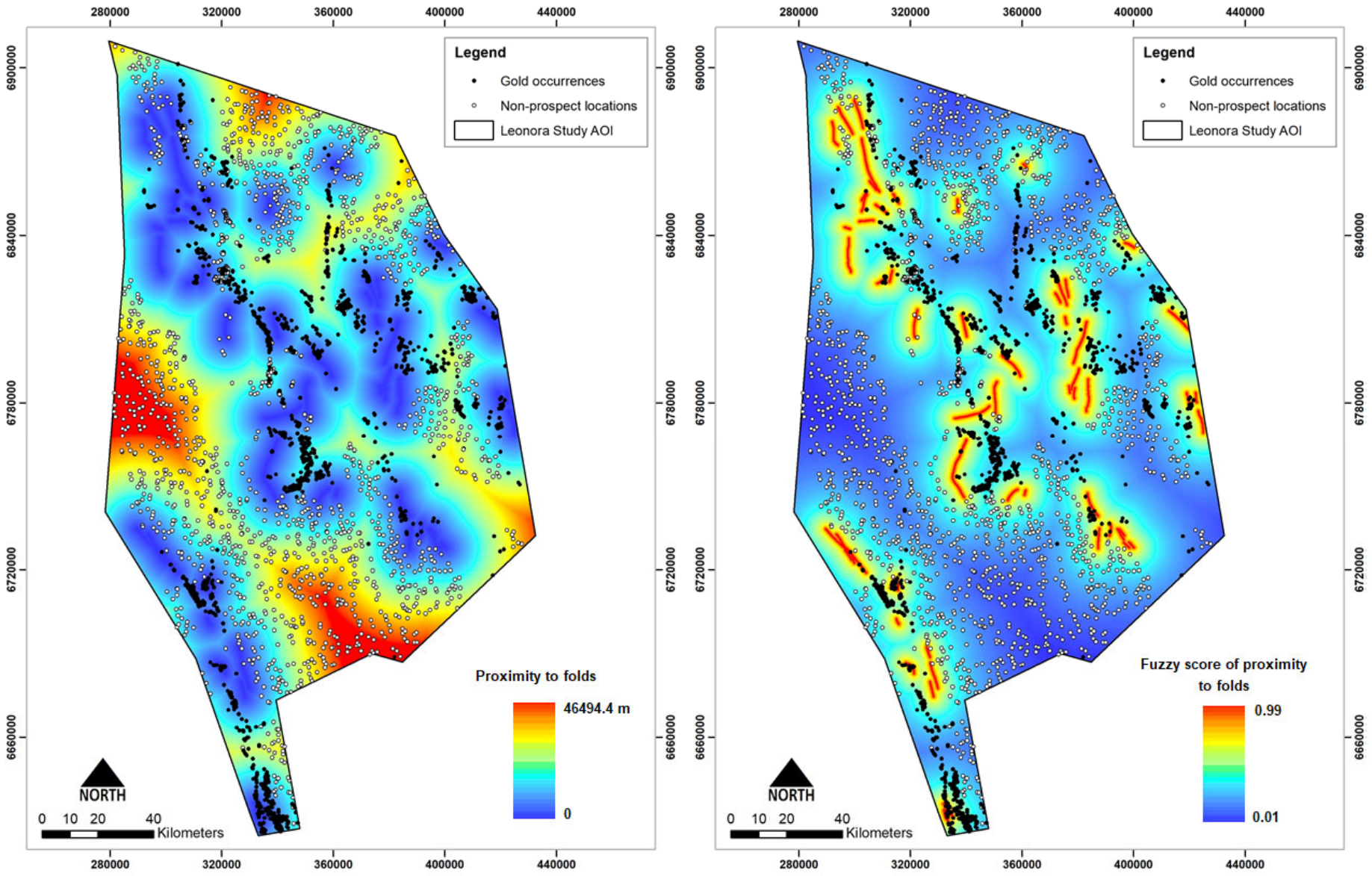

Figure S26. Predictor maps used in this study, part 22: (a) proximity to fold hinges, and (b) proximity to fold hinges, continuously weighted.

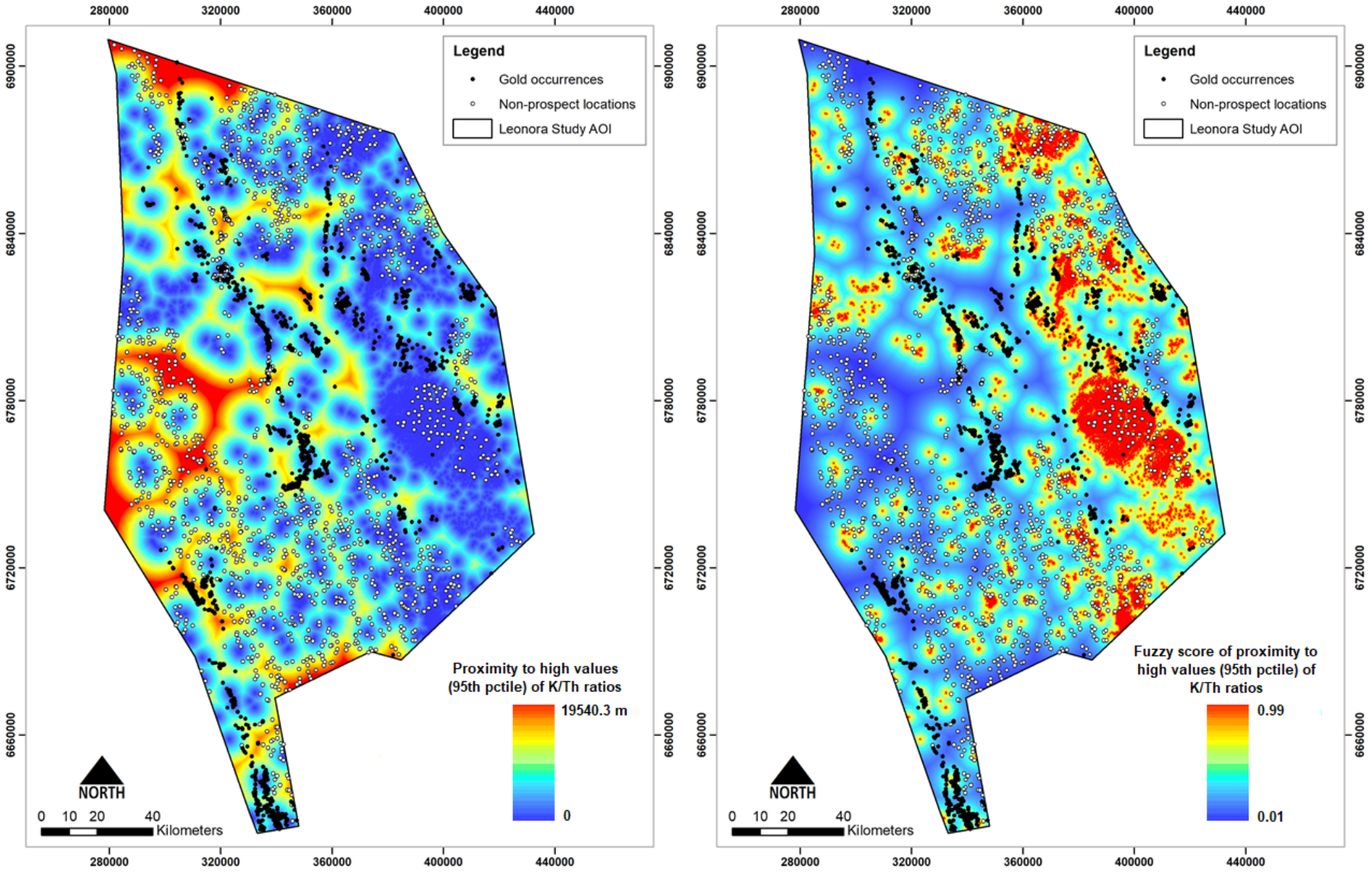

Figure S27. Predictor maps used in this study, part 23: (a) proximity to domains of high K/Th values (≥95th percentile), and (b) proximity to domains of high K/Th values (≥95th percentile), continuously weighted.

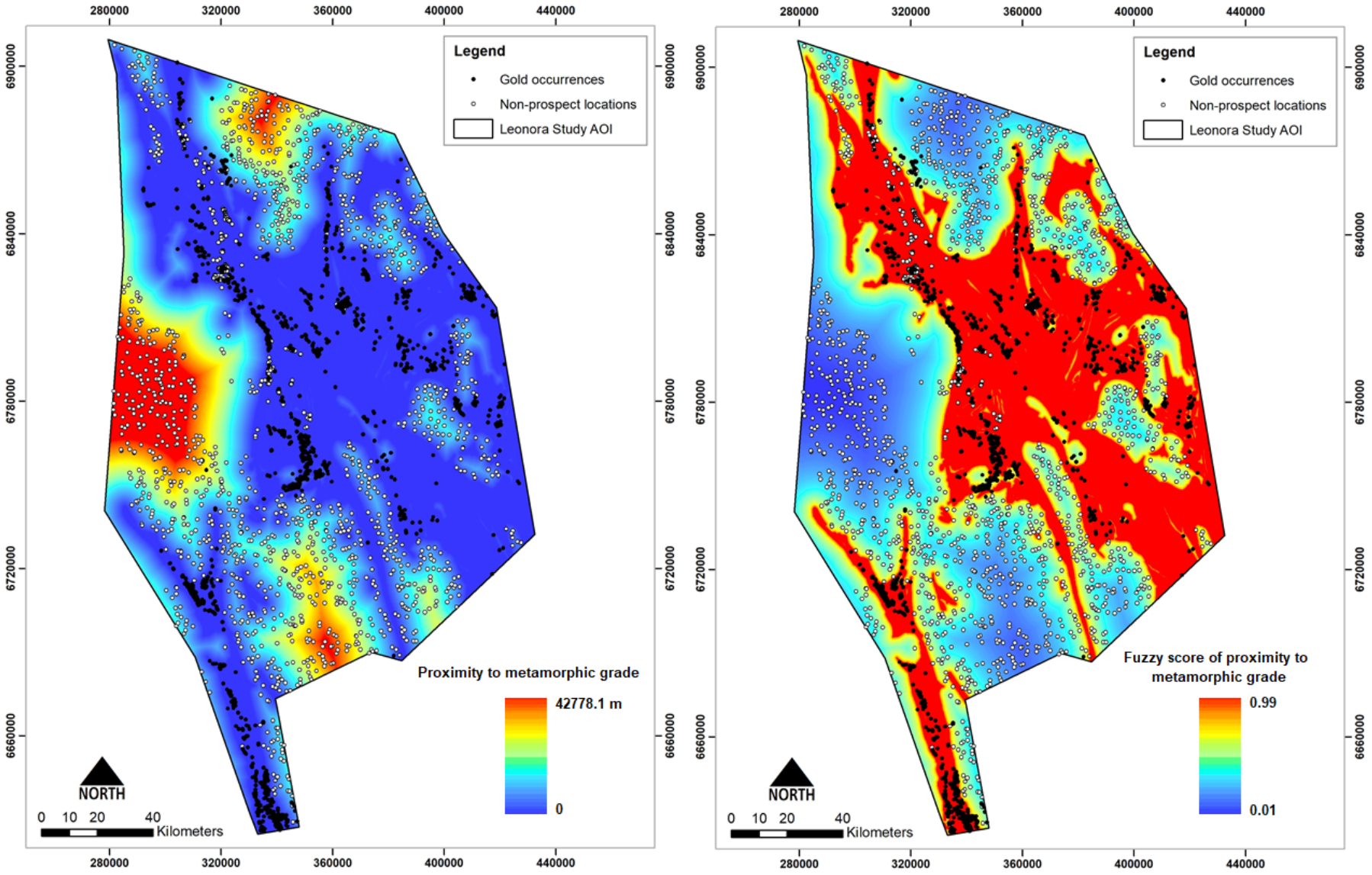

Figure S28. Predictor maps used in this study, part 24: (a) proximity to domains of favorable metamorphic grade, and (b) proximity to domains of favorable metamorphic grade, continuously weighted.

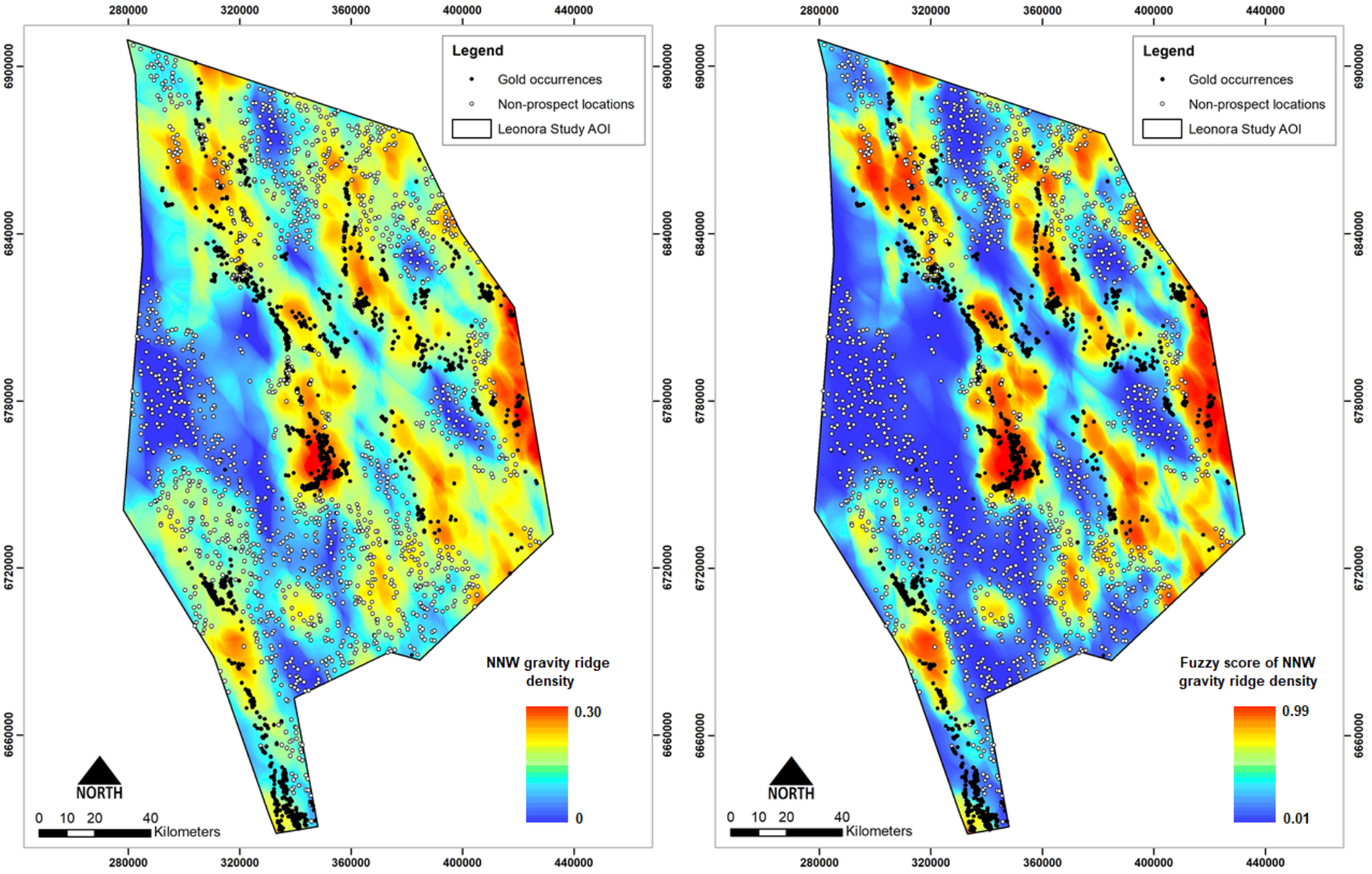

Figure S29. Predictor maps used in this study, part 25: (a) density of NNW-SSE-striking gravity ridges, and (b) density of NNW-SSE-striking gravity ridges, continuously weighted.

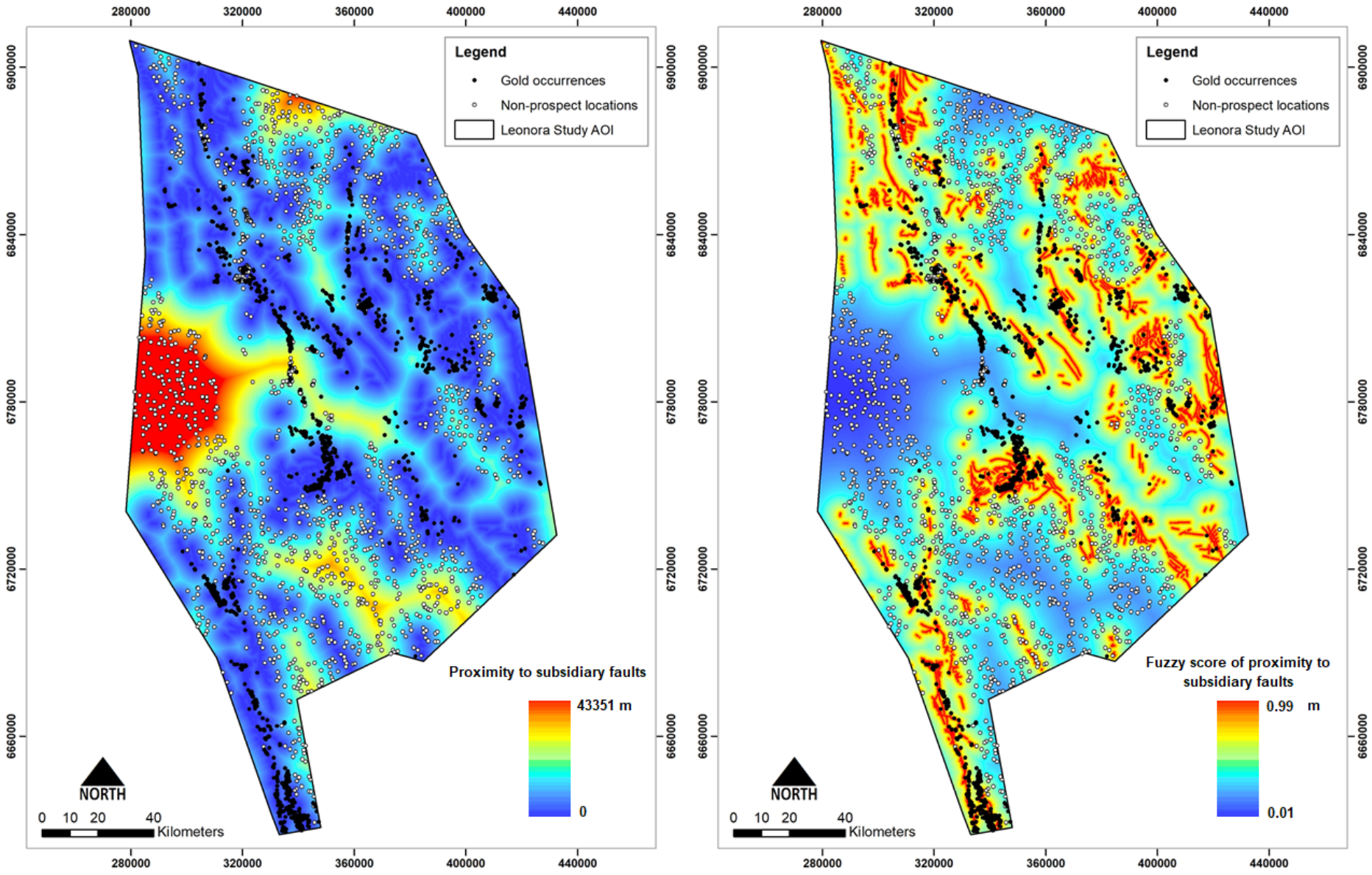

Figure S30. Predictor maps used in this study, part 26: (a) proximity to subsidiary faults, and (b) proximity to subsidiary faults, continuously weighted.

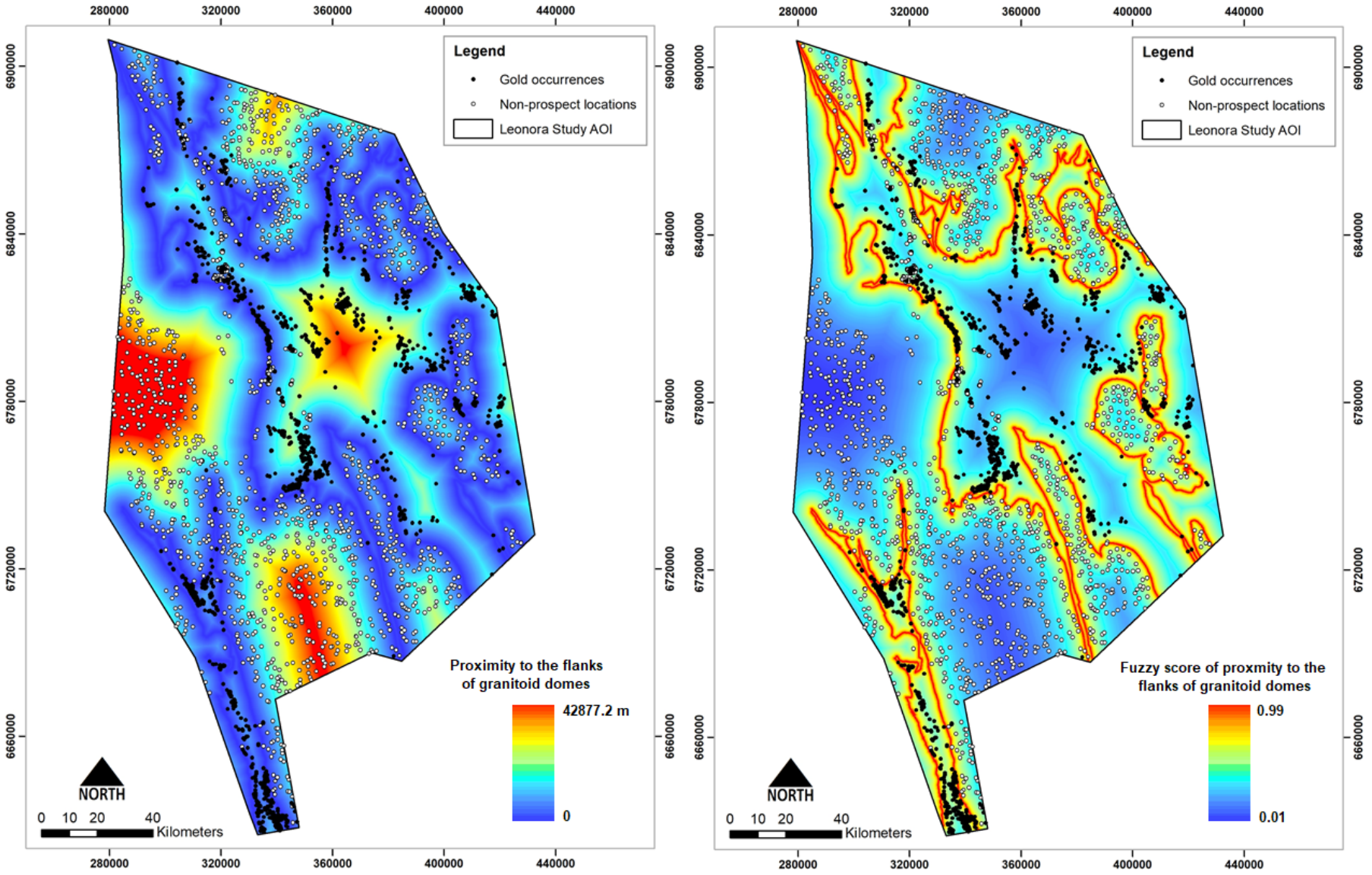

Figure S31. Predictor maps used in this study, part 27: (a) proximity to flanks of granitoid bodies, and (b) proximity to flanks of granitoid bodies, continuously weighted.

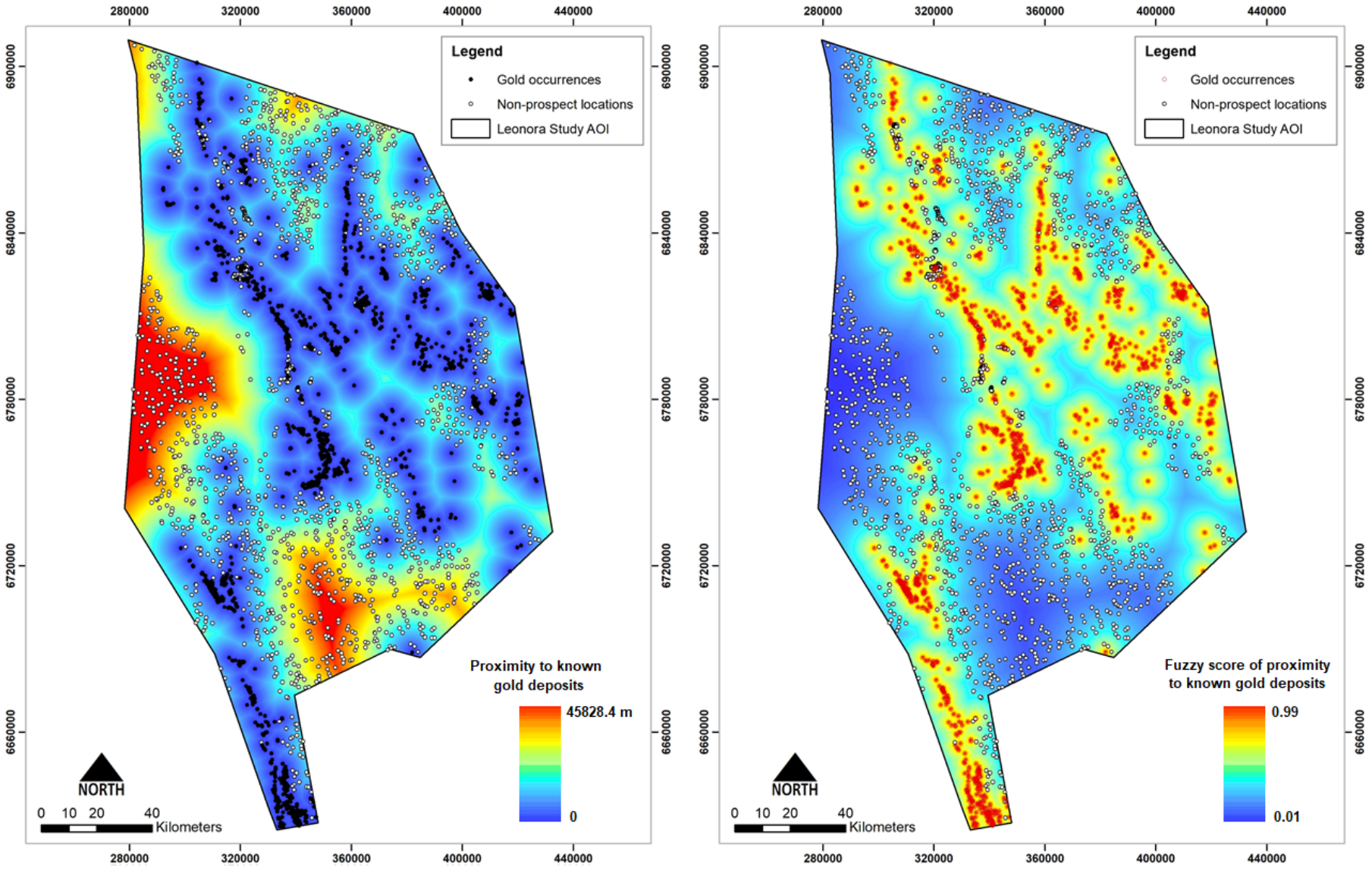

Figure S32. Predictor maps used in this study, part 28: (a) proximity to known gold occurrences, and (b) proximity to known gold occurrences, continuously weighted.

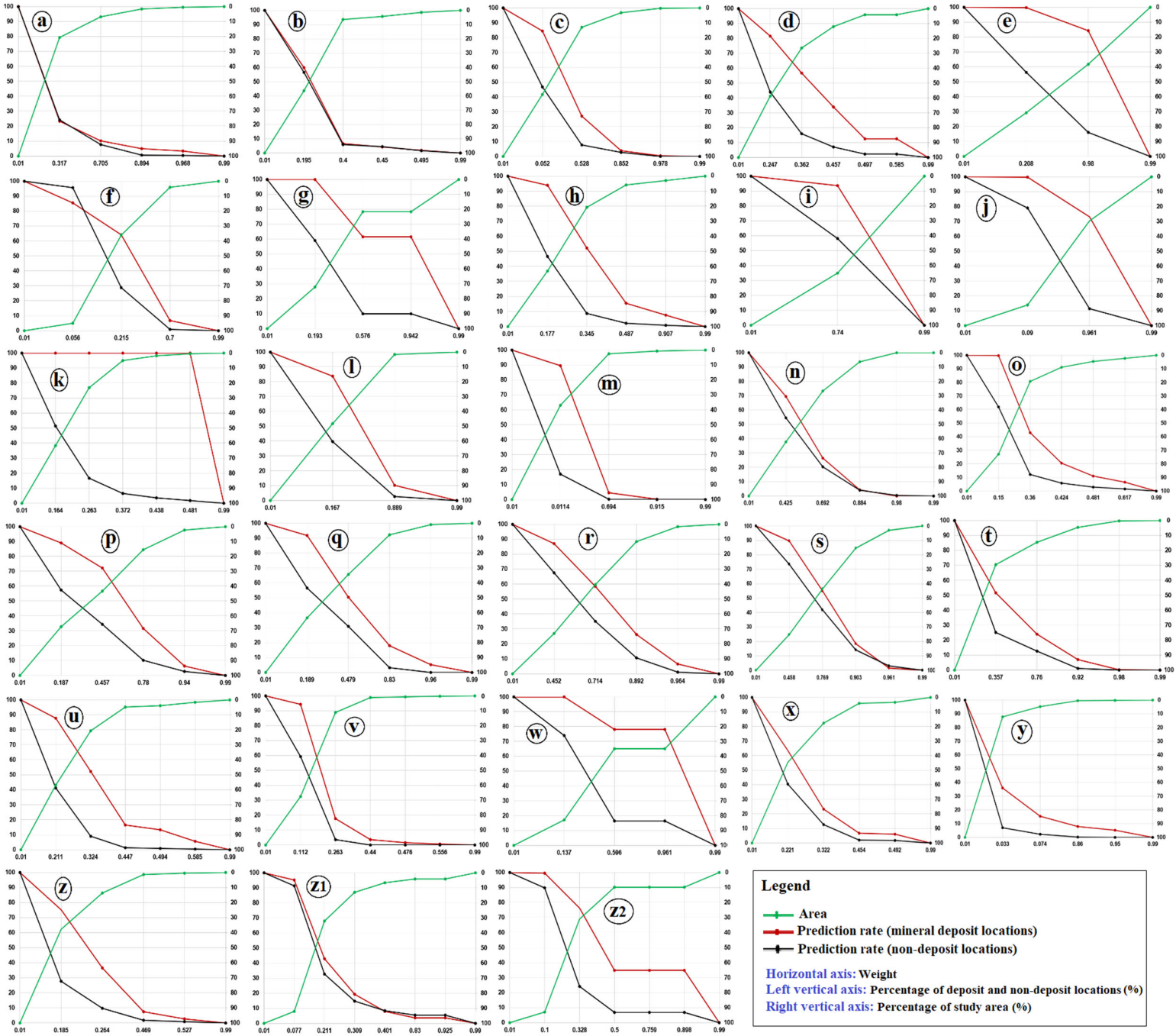

Figure S33. Improved prediction-area plots for the predictor maps used in this study: (a) density of Proterozoic dolerite dykes, (b) proximity to Proterozoic dolerite dykes, (c) density of principal faults, (d) proximity to principal faults, (e) proximity to greenstone belts, (f) proximity to siliciclastic and sedimentary rocks, (g) proximity to mafic–ultramafic volcanic rocks, (h) proximity to 'high mag units', (i) proximity to felsic to intermediate volcanic rocks, (j) proximity to regional gravity highs, (k) proximity to known gold occurrences, (l) proximity to internal granitoids, (m) proximity to basement granitoids, (n) proximity to domains of juvenile crust, (o) proximity to areas of demagnetization, (p) density of ENE-WSW-striking gravity ridges, (q) density of NNW-SSE-striking gravity ridges, (r) density of ENE-WSW-striking gravity lineaments, (s) density of NNW-SSE-striking gravity lineaments, (t) density of principal fault intersections, (u) proximity to subsidiary faults, (v) proximity to fold hinges, (w) proximity to domains of favorable metamorphic grade, (x) proximity to flanks of granitoid bodies, (y) density of lithological contacts, (z) proximity to lithological contacts, (Z1) proximity to domains of high K/Th values, and (Z2) proximity to remotely sensed alteration systems.

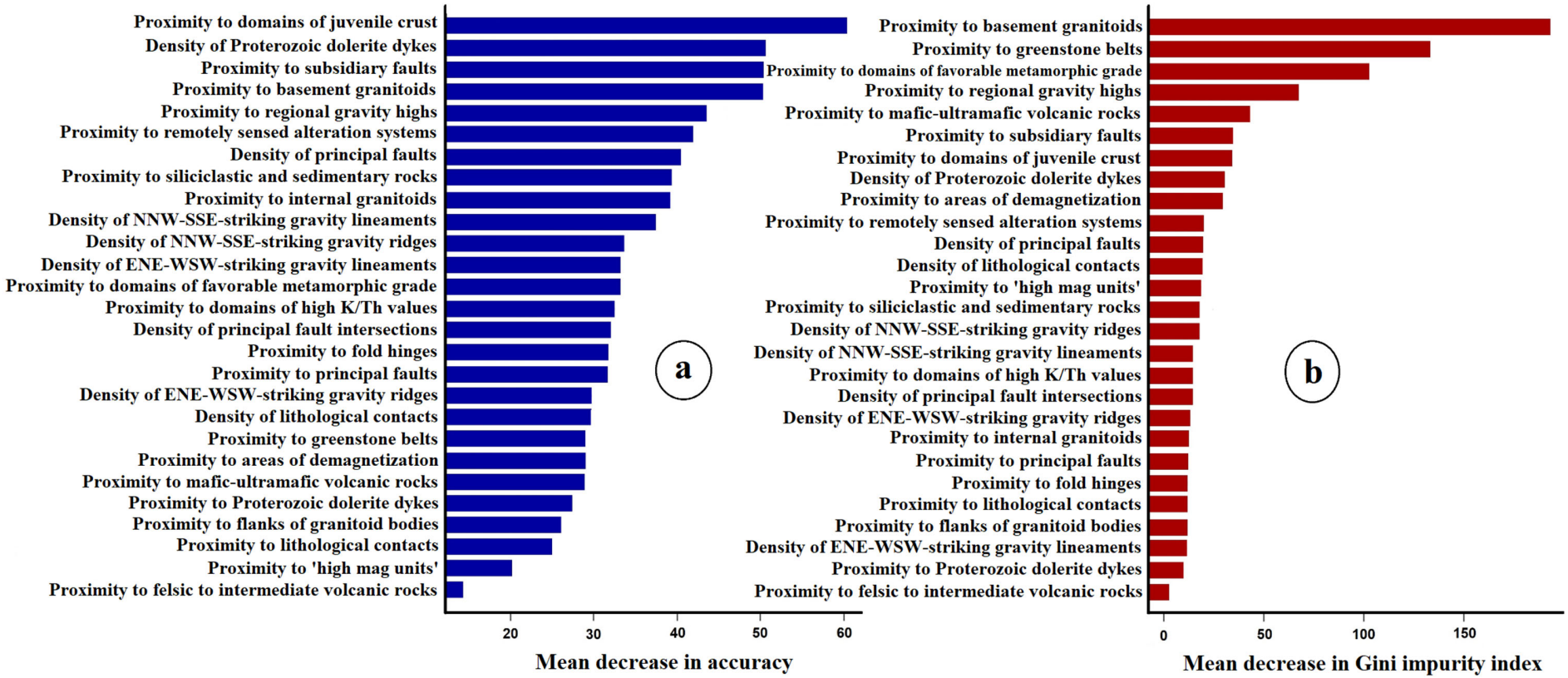

Figure S34. Measure of predictor variable importance derived by RF technique: (a) mean decrease in accuracy, and (b) mean decrease in Gini impurity index.

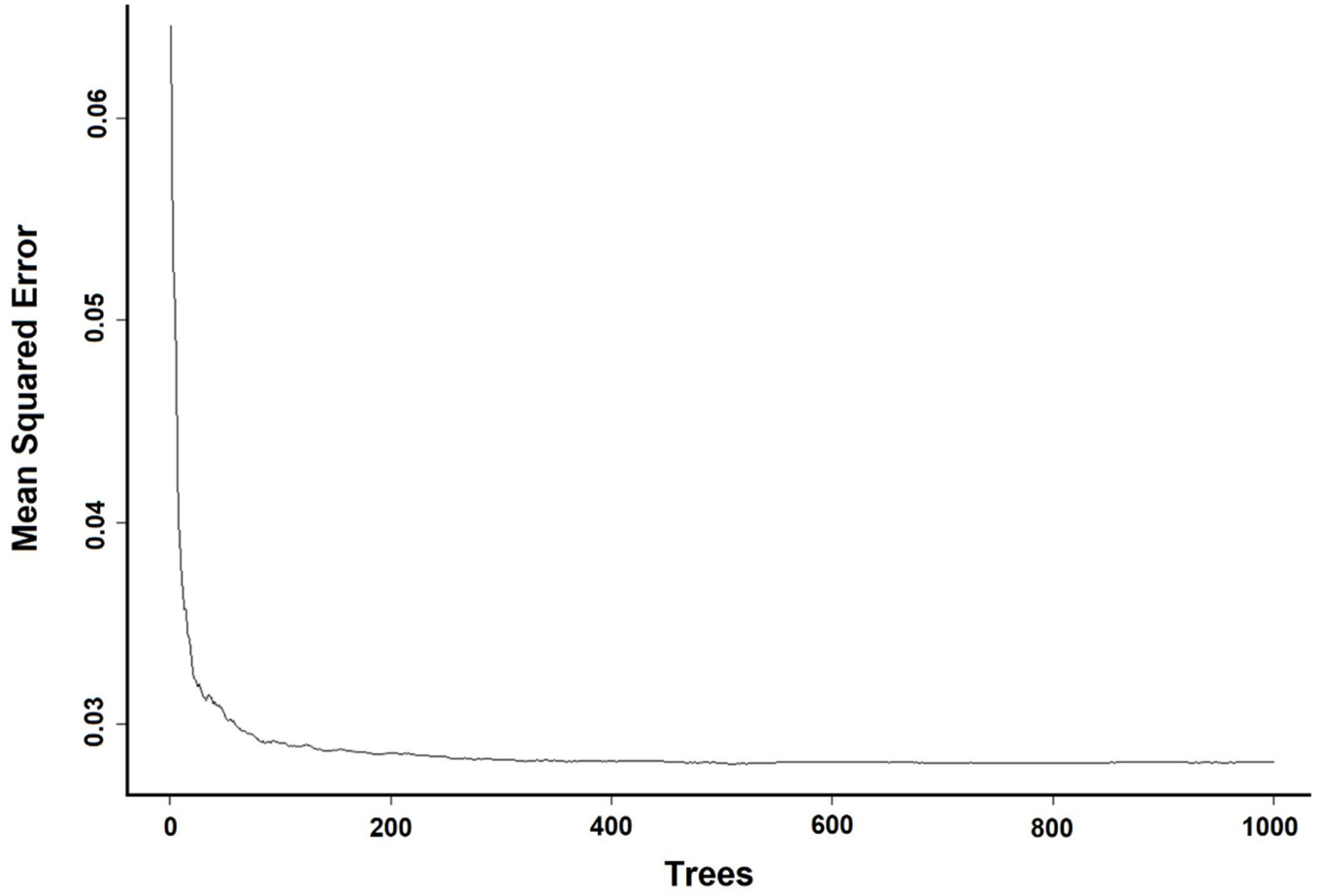

Figure S35. Evolution of mean squared error curve for exploration evidential data utilized for training the RF potential model.

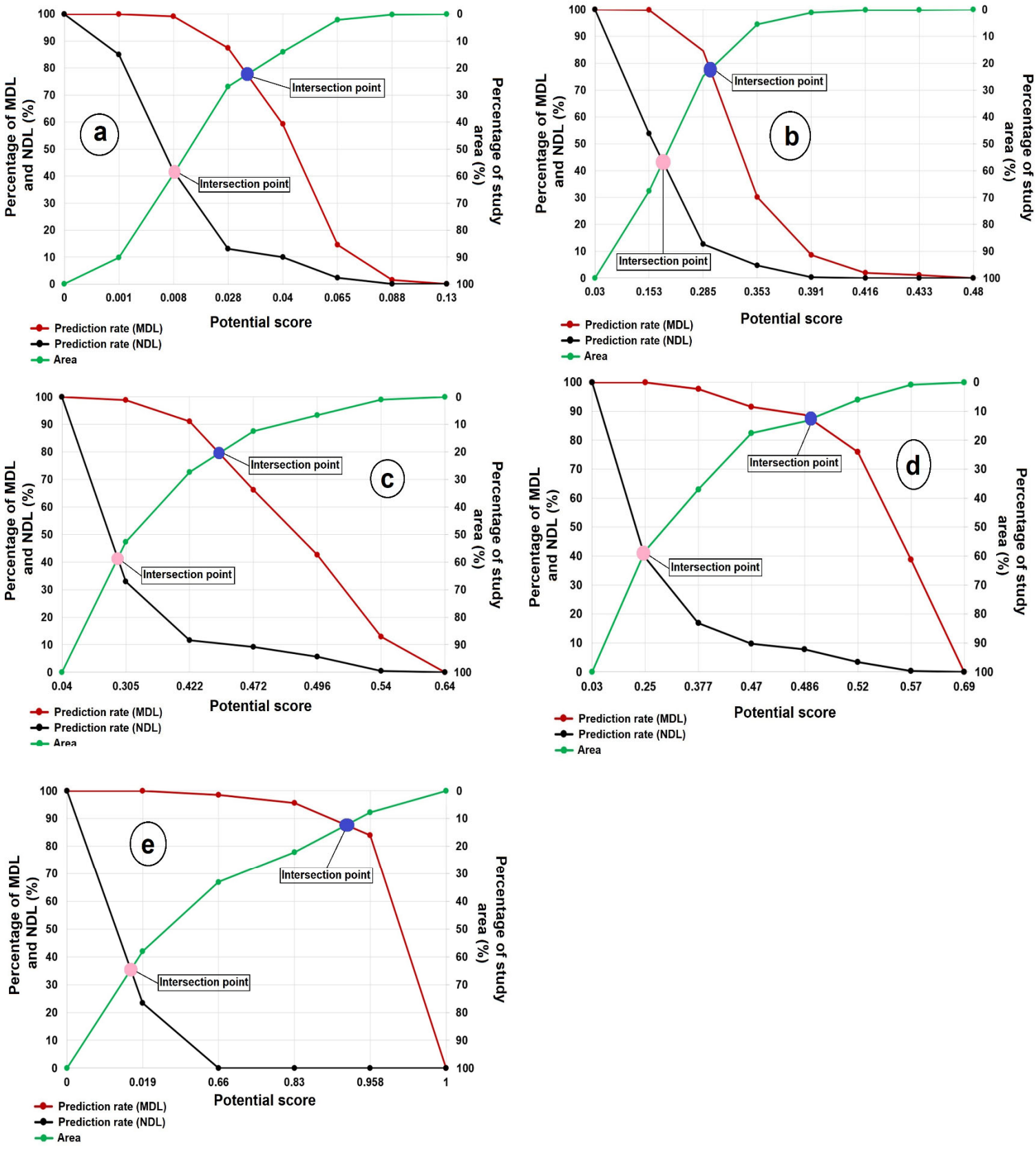

Figure S36. Improved prediction-area plot for the mineral potential models generated in this study: (a) fuzzy gamma, (b) geometric average, (c) improved index overlay, (d) BWM-SAW, and (e) RF.

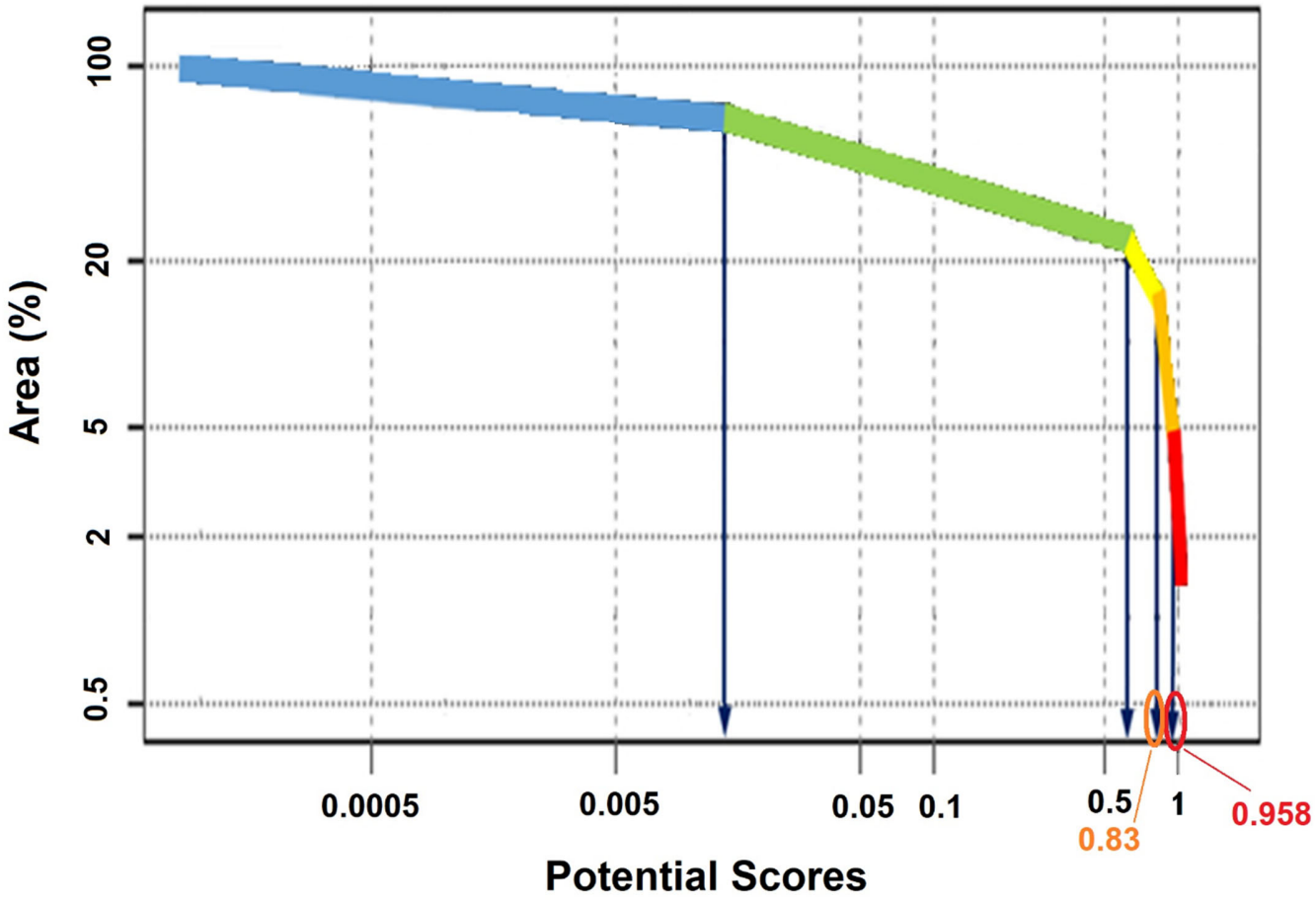

Figure S37. Concentration-area fractal plot for the superior RF mineral potential model.

Table S1. Others-to-worst pairwise comparison vector based on the O_p index.

Decision criteria (predictor maps)	Preference of all other decision criteria over the worst decision criterion
$DC_{W\,(28)}$	1
DC_2	5
DC_3	5
DC_4	5
DC_5	5
DC_6	5
DC_7	5
DC_8	5
DC_9	4
DC_{10}	4
DC_{11}	4
DC_{12}	4
DC_{13}	4
DC_{14}	3
DC_{15}	3
DC_{16}	3
DC_{17}	3
DC_{18}	3
DC_{19}	3
DC_{20}	3
DC_{21}	3
DC_{22}	3
DC_{23}	2
DC_{24}	2
DC_{25}	2
DC_{26}	2
DC_{27}	2
$DC_{B\,(1)}$	9

Table S2. Best-to-others pairwise comparison vector based on the O_p index.

Decision criteria (predictor maps)	$DC_{B\,(1)}$	DC_2	DC_3	DC_4	DC_5	DC_6	DC_7	DC_8	DC_9	DC_{10}	DC_{11}	DC_{12}	DC_{13}	DC_{14}	DC_{15}	DC_{16}	DC_{17}	DC_{18}	DC_{19}	DC_{20}	DC_{21}	DC_{22}	DC_{23}	DC_{24}	DC_{25}	DC_{26}	DC_{27}	$DC_{W\,(28)}$
Preference of the best decision criterion over all other decision criteria	1	2	2	2	2	2	3	3	3	3	3	3	3	3	3	4	4	4	4	4	5	5	5	5	5	5	5	9

Table S3. Optimal weights (W^*) derived from the BWM approach.

Competent Predictor Maps	W^*	ξ^*
Proximity to known gold occurrences (DC_1)	0.100	0.009
Proximity to regional gravity highs (DC_2)	0.054	
Proximity to basement granitoids (DC_3)	0.054	
Proximity to greenstone belts (DC_4)	0.054	
Proximity to domains of favorable metamorphic grade (DC_5)	0.054	
Proximity to mafic–ultramafic volcanic rocks (DC_6)	0.054	
Proximity to subsidiary faults (DC_7)	0.054	
Proximity to remotely sensed alteration systems (DC_8)	0.054	
Proximity to 'high mag units' (DC_9)	0.036	
Proximity to principal faults (DC_{10})	0.036	
Proximity to lithological contacts (DC_{11})	0.036	
Density of ENE-WSW-striking gravity ridges (DC_{12})	0.036	
Proximity to internal granitoids (DC_{13})	0.049	
Density of principal faults (DC_{14})	0.022	
Proximity to siliciclastic and sedimentary rocks (DC_{15})	0.022	
Proximity to areas of demagnetization (DC_{16})	0.022	
Proximity to fold hinges (DC_{17})	0.022	
Proximity to felsic to intermediate volcanic rocks (DC_{18})	0.022	
Density of NNW-SSE-striking gravity ridges (DC_{19})	0.022	
Density of ENE-WSW-striking gravity lineaments (DC_{20})	0.036	
Density of principal fault intersections (DC_{21})	0.036	
Proximity to flanks of granitoid bodies (DC_{22})	0.036	
Density of lithological contacts (DC_{23})	0.014	
Density of NNW-SSE-striking gravity lineaments (DC_{24})	0.014	
Proximity to domains of juvenile crust (DC_{25})	0.014	
Proximity to domains of high K/Th values (DC_{26})	0.016	
Proximity to Proterozoic dolerite dykes (DC_{27})	0.018	
Density of Proterozoic dolerite dykes (DC_{28})	0.010	